# Human iPSC-Based Model Reveals NOX4 as Therapeutic Target in Duchenne Cardiomyopathy

(Short Title: Overexpression of NOX4 in DMD CMs induced cell death)

Robin Duelen[1], Domiziana Costamagna[1,2], Guillaume Gilbert[3], Liesbeth De Waele[4], Nathalie Goemans[4], Kaat Desloovere[2], Catherine M. Verfaillie[5], Karin R. Sipido[3], Gunnar M. Buyse[4] and Maurilio Sampaolesi[1,6,*]

[1]*Translational Cardiomyology, Stem Cell and Developmental Biology, Dept. of Development and Regeneration, KU Leuven, 3000 Leuven, Belgium*

[2]*Research Group for Neurorehabilitation, Dept. of Rehabilitation Sciences, KU Leuven, 3000 Leuven, Belgium*

[3]*Experimental Cardiology, Dept. of Cardiovascular Sciences, KU Leuven, 3000 Leuven, Belgium*

[4]*Pediatric Neurology, University Hospitals Leuven, Dept. of Development and Regeneration, KU Leuven, 3000 Leuven, Belgium*

[5]*Stem Cell Institute Leuven, Stem Cell and Developmental Biology, Dept. of Development and Regeneration, KU Leuven, 3000 Leuven, Belgium*

[6]*Division of Human Anatomy, Dept. of Public Health, Experimental and Forensic Medicine, University of Pavia, 27100 Pavia, Italy*

[*]Corresponding author: Prof. Dr. Maurilio Sampaolesi

Translational Cardiomyology Lab

KU Leuven, Herestraat 49 – O&N4 – bus 804

3000 Leuven, Belgium

Phone: 0032 16373132

Fax: 0032 16330294

Email: *maurilio.sampaolesi@kuleuven.be*

# GRAPHICAL ABSTRACT

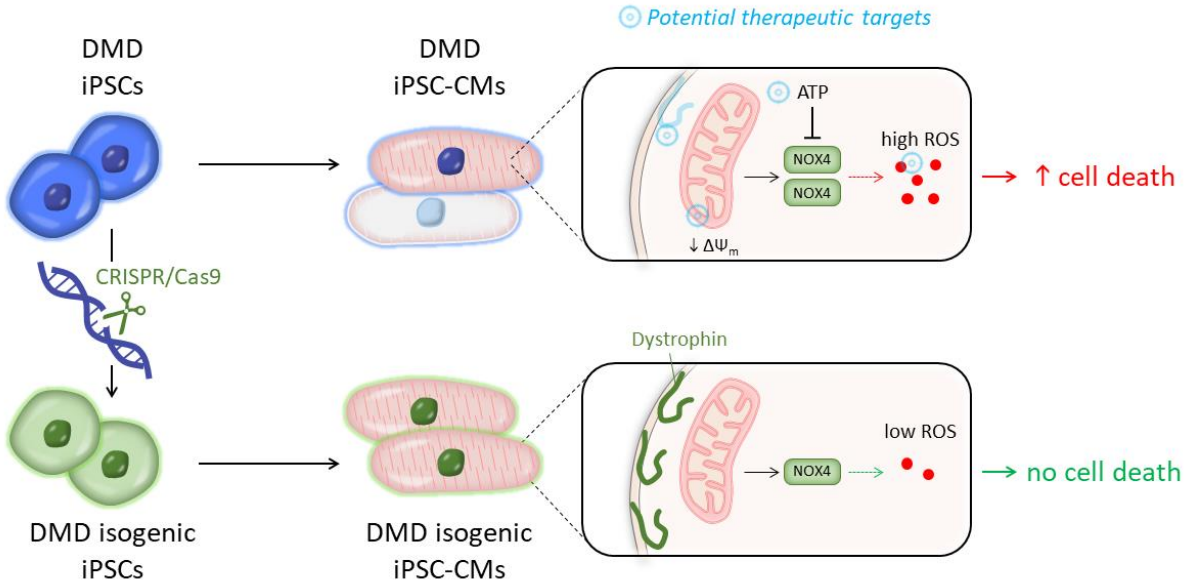


**The use of human induced pluripotent stem cell-derived cardiomyocytes (iPSC-CMs) from Duchenne muscular dystrophy (DMD) patients to model cardiomyopathic features in DMD and unravel novel pathological mechanistic insights.** DMD iPSC-CMs showed accelerated cell death, caused by increased intracellular reactive oxygen species (ROS) levels. By intervention at different target sites, beneficial effects on the mitochondrial membrane potential ($\Delta\Psi_m$) and the expression and ROS-producing activity of the cardiac-specific NADPH-oxidase 4 isoform (NOX4) were observed, resulting in an increased cell survival and function of DMD iPSC-CMs.

# ABSTRACT

Duchenne muscular dystrophy (DMD) is an X-linked progressive muscle disorder, caused by mutations in the *Dystrophin* gene. Cardiomyopathy is one of the major causes of early death. In this study, we used DMD patient-specific induced pluripotent stem cells (iPSCs) to model cardiomyopathic features in DMD and unravel novel pathological mechanistic insights. Cardiomyocytes (CMs) differentiated from DMD iPSCs showed enhanced premature cell death, due to significantly elevated intracellular reactive oxygen species (ROS) concentrations, as a result of depolarized mitochondria and high NADPH oxidase 4 (NOX4) protein levels. Genetic correction of *Dystrophin* through CRISPR/Cas9 editing restored normal ROS levels. Application of ROS reduction by N-acetyl-L-cysteine (NAC), partial Dystrophin re-expression by ataluren (PTC124) and enhancing mitochondrial electron transport chain function by idebenone improved cell survival of DMD iPSC-CMs. We show applications that could counteract the detrimental oxidative stress environment in DMD iPSC-CMs by stimulating adenosine triphosphate (ATP) production. ATP could bind to the ATP-binding domain in the NOX4 enzyme, and we demonstrate that ATP resulted in partial inhibition of the NADPH-dependent ROS production of NOX4.

Considering the complexity and the early cellular stress responses in DMD cardiomyopathy, we propose to target ROS production and prevent the detrimental effects of NOX4 on DMD CMs as a promising therapeutic strategy.


**Keywords:** Duchenne muscular dystrophy, cardiomyopathy, iPSC modeling, CRISPR/Cas9, NADPH oxidase NOX4.

**Teaser:** Increased NOX4 activity in DMD iPSC-CMs could be counteracted by idebenone-stimulated ATP production.

# INTRODUCTION

The shortage of human cardiac cell sources has challenged cardiovascular disease modeling and drug development. The generation of functional cardiomyocytes (CMs) differentiated from human induced pluripotent stem cells (iPSCs) overcomes current limitations and offers an extraordinary platform to develop iPSC-based models to study the genetic disease phenotype of cardiomyopathic pathologies *in vitro* (*1*, *2*).

Mutations in the *Dystrophin* gene cause the X-linked disorder Duchenne muscular dystrophy (DMD), the most common and severe phenotype among the muscular dystrophies (*3*). Most DMD patients develop adverse myocardial remodeling and chronic cardiomyopathy, a major cause of morbidity and early mortality (*4*). With current standards of care, the median life expectancy at birth in DMD seems to have improved considerably during the last decades, ranged between 21.0 and 39.6 years (*5*).

The Dystrophin protein has a crucial role during muscle contraction and stretch. Loss of function or absence lead to myocyte sarcolemma instability during contraction-relaxation cycles, making myocytes more susceptible to stretch-induced damage and necrosis (*6*). The signaling-mediated role of Dystrophin and the associated dystrophin glycoprotein complex is not yet fully understood (*7*). The pathophysiological role of Dystrophin in the heart is poorly defined and little is known about the earliest stages of DMD cardiomyopathy. Multiple pathways are involved including dysregulation of calcium ($Ca^{2+}$) homeostasis, oxidative stress, inflammation and functional ischemia.

Oxidative stress is involved in the pathogenesis of heart failure. However, clinical trials using antioxidants have shown limited success (*8*, *9*). Nicotinamide adenine dinucleotide phosphate (NADPH) oxidase (NOX) family enzymes generate reactive oxygen species (ROS) in a highly regulated manner, modulating several physiological aspects such as host defense, posttranslational processing of proteins, cellular signaling, regulation of gene expression and

cell differentiation (*10, 11*). However, NOX family enzymes also contribute to a wide range of pathological processes, in particular cardiovascular diseases (*12-16*). The NOX4 isoform is predominantly expressed in CMs, although the precise location remains controversial. It is constitutively active at low level (*17*), inducing cardioprotective effects under chronic stress (*18*). The exact role of NOX4 in CMs is still not clear, even though high levels of NOX4 could have severe detrimental effects (*12-16*). Targeting NOX isoforms may be a useful therapeutic strategy. Therefore, there has been significant focus on the potential role of ROS-generating NOX isoform proteins in the pathogenesis of DMD (*14, 15, 19*).

Several innovative therapeutic approaches focus on targeting the primary defect such as restoring the function or expression of Dystrophin through exon skipping (*20*), ribosomal read-through technology (*21*), as well as gene (*22*) and cell therapy (*23*). Recent technological breakthroughs in genome editing successfully enabled the correction of the genetic mutation (*24, 25*). In addition, compounds targeting downstream pathophysiology are under investigation in clinical trials (*26*). Idebenone (2,3-dimethoxy-5-methyl-6-(10-hydroxy)decyl-1,4-benzoquinone), a synthetic analogue of coenzyme $Q_{10}$, has a dual mode-of-action. First, it detoxifies ROS by donating electrons to produce non-toxic reaction products. Second, it donates electrons directly to Complex III of the mitochondrial electron transport chain (ETC), which restores electron flow, proton pumping activity of Complexes III and IV, and adenosine triphosphate (ATP) production by Complex V. Phase 2 and phase 3 randomized placebo-controlled trials have demonstrated a beneficial role of idebenone in DMD patients (*27, 28*).

In this study, we used DMD patient-specific iPSC-derived CMs (iPSC-CMs) to model cardiomyopathic features in DMD and to explore pathological mechanisms. We observed mitochondrial dysfunction and increased concentrations of intracellular ROS in DMD iPSC-CMs, due to significantly increased expression and activity of NOX4. These features were not present in CRISPR/Cas9 genetically corrected DMD isogenic iPSC-CMs. Additionally, by

administration of the ROS scavenger N-acetyl-L-cysteine (NAC), the read-through chemical drug ataluren (PTC124) or the synthetic benzoquinone idebenone to differentiated DMD iPSC-CMs, we observed beneficial outcomes regarding cell survival and function. Interestingly, idebenone showed superior improvements compared to NAC and PTC124 alone or in combination. In addition, our data indicated that idebenone counteracted the hyperactive ROS-producing activity of the cardiac-specific NOX4 isoform through a mechanism mediated by ATP production that could reduce NOX4 activity, resulting in an improved contractile function.

In conclusion, using DMD patient-derived iPSCs, we established an *in vitro* model to recapitulate DMD heart disease phenotypes and to study novel molecular disease mechanisms that might become interesting therapeutic targets for cardiomyopathy in DMD patients.

# RESULTS

## *Generation of Integration-Free DMD iPSCs*

To obtain an unlimited cell source of CMs, recapitulating aspects of a single-gene disease phenotype, iPSC lines were generated from human dermal fibroblasts (hFs) and human peripheral blood mononuclear cells (hPBMCs) obtained from DMD patients with known *Dystrophin* mutations (Table S1). Somatic cells were reprogrammed towards a pluripotent state using the integration-free Sendai virus (SeV) vectors (Fig. S1A-C), which expressed the OSKM (OCT3/4, SOX2, KLF4 and c-MYC) pluripotency markers. Subcutaneously injected DMD iPSC lines into immunodeficient mice displayed teratoma formation, successfully showing the differentiation capacity into all three developmental germ layers (ectoderm, mesoderm and endoderm; Fig. S1D-E). Furthermore, detailed pluripotency analysis for related genes and proteins is given in Supplemental Information (Fig. S2A-B). Three human control iPSC lines were used, generated from healthy donors with no neuromuscular disorders (Table S1).

## *CRISPR/Cas9-Mediated Correction of Nonsense Mutation in* Dystrophin *Gene*

Additionally, we created an isogenic control line to exclude genetic background variability. The isogenic control line was generated using CRISPR/Cas9 technology from the DMD iPSC patient line, characterized by a genetic point mutation in exon 35 (c.4,996C > T; p.Arg1,666X) of the *Dystrophin* gene, resulting in a premature stop codon and consequently in the complete absence of a functional Dystrophin protein (Fig. 1A). To restore full-length expression of the *Dystrophin* gene, two 20-nucleotide single-guide RNAs (sgRNAs) were designed to induce Cas9-mediated double-stranded breaks (DSB) in the genomic DNA of the Dystrophin-deficient iPSCs (Fig. 1B). SgRNA specificity and CRISPR/Cas9 DSB cutting were evaluated in HEK293T cells by the appearance of non-homologous end joining (NHEJ) events after transfection of the sgRNA-Cas9 plasmids (Fig. S3A-B). Cas9-mediated genome editing was

148 performed via homology-directed repair (HDR), using a plasmid-based donor repair template
149 with homology arm regions for the *Dystrophin* gene exon of interest, in order to substitute the
150 premature stop codon into the original amino acid codon for arginine (Fig. 1B). Sequencing
151 analysis of exon 35 of the *Dystrophin* gene confirmed CRISPR/Cas9-mediated genomic
152 correction, further indicated as DMD isogenic control (Fig. 1C). CRISPR/Cas9 off-target
153 events were analyzed based on sequence homology of sgRNAs (Fig. S3C) and detailed
154 comparative genomic hybridization (CGH) molecular karyotyping did not show additional
155 chromosomal abnormalities due to unwanted Cas9-mediated DSB cuts (Fig. S3D). To
156 demonstrate that gene editing did not influence the pluripotency state of the DMD isogenic
157 control, pluripotency genes (*c-MYC, GDF-3, KLF4, NANOG, OCT4, REX1, SOX2* and *hTERT*)
158 and proteins (OCT4, NANOG, SSEA4, SOX2, TRA-1-60 and LIN28) were analyzed in several
159 undifferentiated human pluripotent stem cell (PSC) lines (Fig. S2A-B). Furthermore,
160 immunofluorescent staining showed the expression of Dystrophin protein levels (green) in
161 differentiated DMD iPSC-CMs (cTnT, red and Hoechst, blue) after CRISPR/Cas9 correction
162 (Fig. 1D).
163
164 ***Human iPSC-CMs to Model Diseased Heart Phenotype in DMD***
165 Burridge *et al.* developed a fully chemically defined and small molecule based cardiac
166 differentiation protocol, effective for several human iPSC lines and with high yield of mainly
167 ventricular-like CMs (*29*). Here, we differentiated control and DMD iPSC lines to CMs,
168 according to this monolayer-based cardiac differentiation strategy (*29*), with additional 3D
169 maturation in fibrin-based engineered heart tissue (EHT) constructs (Fig. 2A-B) (*30*). During
170 the early phases of cardiac differentiation, human iPSCs were treated with chemical Wnt
171 signaling mediators (CHIR99021 and IWR-1) to obtain high CM yields (Fig. 2A). Additional
172 3D maturation of iPSC-CMs could significantly increase the expression of the cardiac-specific

maturation isoforms *MYL2* and *TNNI3* (Fig. 2C). Immunostaining of cTnT positive iPSC-CMs additionally matured in 3D EHTs showed structural aligned orientation due to mechanical loading of the flexible microposts compared to classical 2D monolayer-based differentiation systems (Fig. 2D). Importantly, differentiated iPSC-CMs from DMD patients manifested pathologic features of cardiac involvement. They exhibited a significant reduction of the L-type $Ca^{2+}$ current, indicating abnormal $Ca^{2+}$ homeostasis (Fig. 2E), and representative action potential (AP) recordings from DMD iPSC-CMs displayed arrhythmogenic firing pattern including delayed afterdepolarizations (DADs) and oscillatory prepotentials (OPPs; Fig. 2F), as reported in literature by Eisen *et al.* and others (*31*-*36*). Furthermore, detailed patch-clamp recordings at day 24 of differentiation showed significant longer mean action potential duration at 90% repolarization (APD90) of DMD iPSC-CMs compared to control iPSC-CMs (Fig. 2G). Other electrophysiological parameters including AP amplitude, resting membrane potential (RMP), cell capacitance and beating frequency did not show significant differences (Fig. 2H).

***Enhanced Cell Death and Excessive Intracellular ROS Levels in DMD iPSC-CM Cultures***

The absence of Dystrophin protein in differentiated iPSC-CMs from DMD patients (Fig. S4) results in progressive loss of CMs (*6*, *32*). In this study, we wanted to identify novel pathological cues that caused decreased cell survival of DMD iPSC-CMs. We mainly used the DMD iPSC patient line that was characterized by the nonsense mutation in exon 35 (c.4,996C > T; p.Arg1,666X) of the *Dystrophin* gene (DMD #2 in Table S1). This DMD line represents a subgroup of DMD patients (approximately 13%) that is responsive to the read-through chemical drug ataluren (PTC124; Fig. 5A-C). Cell death was examined by flow cytometric analyses, using annexin V and 7-amino-actinomycin D (7AAD). DMD iPSC-CMs underwent accelerated cell death (DMD, early apoptosis: 15 ± 1% and late apoptosis: 33 ± 6%) compared to corresponding DMD isogenic (isoC, respectively 3 ± 0% and 7 ± 1%) and healthy controls (HC,

respectively 5 ± 0% and 15 ± 1%; Fig. 3A and Fig. S6A, *left panels*). A remarkable percentage of DMD iPSC-CMs had high intracellular ROS concentrations (DMD, $[ROS]^{high}$: 68 ± 2%) compared to controls (isoC, $[ROS]^{high}$: 46 ± 3% and HC, $[ROS]^{high}$: 41 ± 1%; Fig. 3B and Fig. S6A, *middle panels*). Moreover, the intracellular ROS content (mean fluorescence intensity, MFI) in DMD iPSC-CMs was significantly higher (DMD, 28,924 ± 1,864 vs. isoC, 5,276 ± 254 and vs. HC, 6,198 ± 213; Fig. 3C and Fig. S6A, *right panels*). Upon treatment with NAC and PTC124 (alone or in combination) as well with idebenone, DMD iPSC-CMs showed increased cell survival (DMD early apoptosis, NAC: 7 ± 1%, PTC124: 8 ± 1%, NAC+PTC124: 9 ± 1% and idebenone: 3 ± 0% vs. untreated: 15 ± 1% and DMD late apoptosis, NAC: 25 ± 2%, PTC124: 24 ± 2%, NAC+PTC124: 21 ± 2% and idebenone: 5 ± 1% vs. untreated: 33 ± 6%; Fig. 3A and Fig. S6A, *left panels*) and reduced intracellular ROS levels (DMD $[ROS]^{high}$, NAC: 36 ± 4%, PTC124: 41 ± 11%, NAC+PTC124: 48 ± 7% and idebenone: 52 ± 3% vs. untreated: 68 ± 2%; Fig. 3B and Fig. S6A, *middle panels*) compared to untreated DMD iPSC-CMs. The specificity of the drug effect on the CM death and on the intracellular ROS levels of the experimental groups is shown in Supplemental Information (Fig. S7A-D). Taken together, these results show increased intracellular ROS levels in DMD iPSC-CMs. Interestingly, NAC, PTC124 and idebenone had beneficial effects on the cell survival, although idebenone addition exhibited superior effects on DMD iPSC-CM cultures.

***Dystrophin-Deficient iPSC-CMs Are Characterized by Depolarized Mitochondria***

DMD pathology is accompanied by abnormal intracellular $Ca^{2+}$ handling and the accumulation of dysfunctional mitochondria with defective structure (*31-38*). A distinctive feature of early phase cell death is the loss of the membrane potential of active mitochondria ($\Delta\Psi_m$) (*39*). Here, the carbocyanine compound JC-1, a fluorescent voltage-sensitive dye with membrane-permeant fluorescent lipophilic cationic properties (*40*), was used to determine $\Delta\Psi_m$ in iPSC-CMs and

mitochondrial health. Consistently with the previously observed accelerated death of untreated DMD iPSC-CMs, these cultures were characterized by mitochondrial depolarization, indicated by the decrease in red (aggregates)/green (monomers) JC-1 fluorescence intensity ratio (DMD, JC-1 aggregates: 31 ± 4% and JC-1 monomers: 68 ± 4%) compared to DMD isogenic (isoC, respectively 71 ± 2% and 28 ± 2%) and healthy controls (HC, respectively 71 ± 1% and 28 ± 2%; Fig. 3D-E and Fig. S6B). Interestingly, the combinatorial treatment of NAC and PTC124 (DMD NAC+PTC124, JC-1 aggregates: 60 ± 4% and JC-1 monomers: 38 ± 3%), as well as idebenone treatment (DMD idebenone, respectively 68 ± 2% and 32 ± 3%) displayed significantly beneficial effects on $\Delta\Psi_m$ with respect to untreated DMD iPSC-CMs (DMD untreated, respectively 31 ± 4% and 68 ± 4%). Furthermore, flow cytometric analyses confirmed a significant increased superoxide production in depolarized mitochondria (DMD, 75 ± 6%) compared to controls (isoC, 22 ± 1% and HC, 30 ± 5%; Fig. 3F and Fig. S6C). No significant differences were observed for mitochondrial content upon the different treatments (Fig. S6D-E). The specificity of the drug effect on $\Delta\Psi_m$ and on the mitochondrial superoxide concentrations of the experimental groups is shown in Supplemental Information (Fig. S8A-D). Taken together, these results indicate dysfunctional depolarized mitochondria in DMD iPSC-CMs, which could lead to excessive ROS leakage. The combined treatment of NAC and PTC124, as well of idebenone to DMD iPSC-CM cultures were able to rescue this condition.

***NOX4 Is Overexpressed in DMD iPSC-CMs***

Several independent studies have reported increased NOX4 expression and activity in chronic heart failure, supporting the clinical relevance, although the role of NOX4 in CMs is still unclear (*12-16*). Here, the NOX2 and NOX4 isoforms, the predominantly expressed members of the ROS-producing NOX family in the heart, were investigated. Gene expression profiles did not reveal differential expression for *NOX2* and accessory regulatory subunits ($p47^{phox}$,

248 *p67$^{phox}$*, and *RAC2* and *RAC3;* Fig. 4A). Interestingly, *NOX4* and its regulatory subunit *p22$^{phox}$*
249 were significantly upregulated in DMD iPSC-CMs. Moreover, DMD iPSC-CMs treated with
250 PTC124 alone or in combination with NAC exhibited decreased *NOX4* and *p22$^{phox}$* gene levels.
251 In contrast, upon idebenone treatment, no reduction was observed in the expression of both
252 genes. Flow cytometric analyses demonstrated a significant increased percentage of NOX4
253 positive DMD iPSC-CMs (DMD, 78 ± 3%) compared to DMD isogenic (isoC, 31 ± 4%) and
254 healthy controls (HC, 29 ± 1%; Fig. 4B-C). The percentage of NOX4 positive DMD iPSC-CMs
255 was reduced upon idebenone treatment (DMD idebenone, 34 ± 4% vs. isoC, 31 ± 4% and vs.
256 HC, 29 ± 1%). The specificity of the drug on the expression of NOX4 among the experimental
257 groups is shown in Supplemental Information (Fig. S9A-B). Western blot analysis confirmed
258 significantly increased protein levels of NOX4 in DMD iPSC-CMs. (Fig. 4D). Upon idebenone
259 addition, DMD iPSC-CMs showed downregulated NOX4 expression like observed in controls.
260 These data demonstrate a significantly increased NOX4 expression in DMD iPSC-CMs that
261 upon treatment with idebenone could be reverted to physiological levels.

262 Additionally, we demonstrated that the NOX4 upregulation in DMD iPSC-CMs (DMD
263 #2 in Table S1) was not a common downstream pathway of cell death. Therefore, we
264 preincubated iPSC-CMs with 1 μM STS for 6 h, a potent cell death inducer (*41*), and did not
265 observe any increase in the NOX4 expression (Fig. S10A-B). Interestingly, by analyzing $\Delta\Psi_m$
266 and the mitochondrial superoxide production in various DMD patient-specific iPSC-CM lines
267 (DMD #2, DMD #5 and DMD #6 in Table S1), we could observe an association between the
268 levels of mitochondrial depolarization and ROS production with the gene and protein levels of
269 NOX4, suggesting a crucial role of NOX4 (Fig. S11A-F).

270

271 ***Idebenone Stimulates ATP Production in Depolarized Mitochondria, Ameliorating NOX4-***
272 ***Mediated ROS Overproduction***

Overall, oxidative stress, in synergy with intracellular $Ca^{2+}$ overload, results in progressive worsening of DMD cardiomyopathy (*7, 37*). We hypothesized that *Dystrophin* gene mutations elicit excessive ROS generation via the mitochondrial ETC of dysfunctional mitochondria and a NOX4-based NADPH-dependent process. To assess whether increased NOX4 could contribute to elevated intracellular ROS concentrations, *NOX4* mRNA levels were transiently degraded by the addition of Antisense LNA GapmeRs to the DMD iPSC-CM cultures (Fig. 5A, *left panel*). Antisense LNA GapmeRs targeting *MALAT1* mRNA were used as positive control (Fig. 5A, *right panel*). Interestingly, transient GapmeR-induced *NOX4* mRNA degradation significantly reduced the NOX4 activity, monitored through changes in NADPH absorption (Fig. 5B) (*42, 43*). DMD iPSC-CMs exhibited significantly elevated NOX4 activity compared to controls (Fig. 5C). However, when idebenone was added to DMD iPSC-CMs, the NOX4 NADPH-dependent ROS production was significantly reduced in isolated mitochondria (Fig. 5C) and the total CM fraction (Fig. S12A). Moreover, idebenone restored ATP levels due to its electron donating property for mitochondrial ETC stimulation (Fig. 5D and Fig. S12B).

Recent studies have identified an ATP-binding motif within NOX4 through which ATP, upon binding, could regulate NOX4 activity (*43*). Adding dose-dependent ATP concentrations to DMD iPSC-CM cultures demonstrated that 2.5 mM ATP had a beneficial effect and significantly reduced ROS production of the NOX4 activity in respect to no ATP addition (Fig. 5E and Fig. S12C). Interestingly, idebenone alone or in combination with 2.5 mM ATP addition did ameliorate the activity of NOX4, in a similar manner, resulting in a significantly decreased NADPH-dependent ROS production compared to untreated DMD iPSC-CMs (Fig. 5F and Fig. S12D). The specificity of idebenone on the ROS-producing activity of NOX4 and on the ATP levels of the experimental groups is shown in Supplemental Information (Fig. S13A-D). These findings reveal an increased mitochondrial ROS-producing NOX4 activity in DMD iPSC-CMs, which was counteracted by idebenone application through ATP.

298

299 ***DMD EHTs Show Improved Contractile Function after Idebenone Administration***

300 In order to assess the amplitude of contraction of 3D EHT constructs, we monitored the
301 micropost deflection movements of the EHT devices as a result of spontaneous contraction of
302 the EHTs attached to the flexible microposts (Fig. 2B). At physiological 1.8 mM $Ca^{2+}$
303 concentrations, the contractile function of untreated DMD iPSC-CM EHTs was significantly
304 lower than untreated EHTs generated from isogenic or healthy iPSC-CMs (Fig. 6A), confirming
305 the validity of the 3D EHT model system for DMD. However, DMD EHTs treated with
306 idebenone exhibited a significantly increased contraction, whereas the combined treatment of
307 idebenone and PTC124 improved even further the contractile function. By incubating DMD
308 EHTs with various $Ca^{2+}$ concentrations (ranging from 0.1 to 2.5 mM), we wanted to analyze
309 the amplitude of contraction of DMD EHTs at physiological $Ca^{2+}$ levels (1.8 mM; dotted line)
310 and higher $Ca^{2+}$ levels (2.5 mM), mimicking the detrimental increased $Ca^{2+}$ environment, as
311 reported in the heart from DMD patients (*35*, *44*, *45*). At physiological $Ca^{2+}$ levels, idebenone
312 had beneficial effects on the contraction of DMD EHTs compared to untreated DMD EHTs,
313 whereas the contractile function of DMD EHTs did not show any improvements upon
314 idebenone administration at 2.5 mM $Ca^{2+}$ concentrations (Fig. 6B). However, the contractile
315 function was significantly improved after the combinatorial treatment of idebenone and
316 PTC124. These data point out the beneficial effect of a combinatorial treatment of idebenone
317 and PTC124, highlighting the importance of targeting simultaneously different aspects of DMD
318 cardiomyopathy in terms of heart functionality.

# DISCUSSION

Human iPSCs have the potential to differentiate in functional cell types that can be used as unlimited cell source of inaccessible tissues to study genetic disorders and, consequently, to gain novel insights in signaling pathways involved in the disease pathology.

In this study, we generated iPSC-based cardiac disease models from sample material of three DMD patients to study the early stages of cardiomyopathy in DMD. Human iPSCs were differentiated towards CMs according to the protocol of Burridge *et al.* (Nature Methods) (*29*) and Breckwoldt *et al.* (Nature Protocols) (*30*). First, human iPSCs were differentiated in a monolayer-based method using a fully chemically defined medium, consisting of the basal medium RPMI 1640, rice-derived recombinant human albumin and L-ascorbic acid 2-phosphate along with small molecule-based induction of differentiation (*29*). L-ascorbic acid 2-phosphate has been shown to enhance cardiac differentiation and maturation through increased collagen production by promoting cardiac progenitor cell proliferation via the MEK-ERK1/2 pathway. Furthermore, L-ascorbic acid 2-phosphate-induced CMs exhibited better sarcomeric organization and enhanced responses of APs and $Ca^{2+}$ transients to β-adrenergic and muscarinic stimulations (*46*). Second, iPSC-CMs were further differentiated in 3D fibrin-based EHT constructs for contractility measurements (*30*). In several cancer-related studies the effect of ascorbic acid on ROS production has been reported (*47, 48*). In these studies, a ROS-scavenger effect was observed after the addition of 1 mM or higher concentrations of ascorbic acid. We used a lower final concentration, suggesting no significant antioxidative effect on ROS levels. Interestingly, Bartsch *et al.* (*49*) demonstrated an ascorbic acid enhanced cardiac differentiation accompanied by an upregulation of the NADPH oxidase isoforms NOX2 and NOX4 at basal expression levels with intracellular physiological ROS concentrations, indicating the suitability of the applied cardiac differentiation methods.

Human iPSC-CMs obtained from DMD patients represent hallmarks of DMD-associated heart complications in *in vitro* cultures. Published studies showed that the lack of Dystrophin in DMD iPSC-CMs resulted in enhanced cell death (*32*), $Ca^{2+}$ handling abnormalities and reduced contractile function (*31, 33-36, 44, 45, 50*). We observed premature cell death of DMD iPSC-CMs due to significantly elevated intracellular oxidative stress levels. Furthermore, detailed characterization demonstrated mitochondrial depolarization and significantly increased NOX4 expression. Whether the abnormally upregulated NOX4 expression and its increased basal rate of ROS production are a direct or indirect consequence of the absence of Dystrophin is currently unknown. Increased Nox4 protein have been found in left ventricular CMs of *mdx* mice, associated with fibrosis and altered functional parameters in the heart (*14*). Deep RNA sequencing of the cardiac transcriptome on explanted human heart samples, obtained from patients suffering from heart failure, indicated extensive alternative splicing of the *NOX4* gene, associated with upregulation of the full-length NOX4 protein (*15*). In consistency with these results, we found a significantly increased expression and activity of the cardiac-specific ROS-producing NOX4 isoform in DMD iPSC-CMs. Dystrophin-deficient CMs are more vulnerable to mechanical stress due to the increased membrane fragility and stretch-induced $Ca^{2+}$ influx, resulting in cell death (*32, 35, 44, 45*). The complexity of the DMD pathology results from the signal amplification systems, with bidirectional cross-talk and positive feed-back loops. ROS generation in response to mechanical forces may originate from diverse sources including mitochondria and NOX isoforms (*12, 13, 16*), or even other oxidase systems (*19, 51, 52*).

To ameliorate the DMD disease phenotype, we applied several therapeutic approaches. We investigated whether NAC, ataluren (PTC124) and idebenone could have beneficial effects on the dystrophic features observed in DMD iPSC-CM cultures. PTC124 drug efficacy analyses were performed only on the DMD iPSC line with the nonsense mutation in exon 35 (c.4,996C

> T; p.Arg1,666X) of the *Dystrophin* gene. This line represents a subgroup of DMD patients (approximately 13%) that is responsive to the read-through chemical drug PTC124, which allowed us to investigate the effects of PTC124 on DMD cardiomyopathy in an *in vitro* iPSC-based disease model. PTC124 is one of the gene-based therapeutic approaches for DMD, although applicable for only a small subgroup of DMD patients with a nonsense mutation (*21*). We demonstrated re-expression of Dystrophin after PTC124 addition in a fraction of differentiating DMD iPSC-CMs. Recently, a phase 3 randomized placebo-controlled trial, evaluating an improvement in the 6-minute walking test after 48 weeks, has been completed (*53*), and a clinical trial to study Dystrophin expression levels in a small cohort of PTC124-treated patients with DMD is currently ongoing. These clinical studies aim at targeting the primary cause of DMD progression.

Nowadays several innovative therapeutic approaches focus on the secondary pathology. In the last decade, researchers have shown growing interest for idebenone as potential treatment for DMD. The precise mechanism by which idebenone exerts its protective effect is still unknown. Yet, idebenone has been reported to protect mitochondria from oxidative damage and boost their impaired function, delaying disease progression of DMD (*27, 28*). Interestingly, given the dual mode-of-action of idebenone (ROS-scavenger function and stimulation of the mitochondrial ETC), we showed that idebenone application exhibited a superior beneficial outcome on DMD iPSC-CMs through increased ATP production that, on its turn, decreased NOX4 activity. The exact mechanism of ATP-mediated inhibition of the NOX4 activity is still unclear.

Recently, an ATP-binding motif within the NOX4 isoform has been identified, suggesting a potential novel mechanism through which NOX4 can be allosterically regulated. During normal respiration, OXPHOS-driven ATP production in the mitochondria binds NOX4 through the ATP-binding domain, keeping the NOX4-produced ROS levels low (*43*). The ATP-

binding motif (AXXXXGKT) (*54*) that resides within the amino acids 534-541 of the C-terminus, is unique to NOX4 (not found in other NOX isoforms) and is conserved in *Homo sapiens, Rattus norvegicus* and *Mus musculus* (*43*). In line with these results, we demonstrated that the addition of idebenone to DMD iPSC-CM cultures increased the intracellular and, more specifically, the mitochondrial ATP concentrations through idebenone-induced ETC stimulation. Moreover, idebenone could significantly reduce the ROS-producing NOX4 activity, assuming the allosterically regulation of NOX4 through ATP. Interestingly, the addition of external ATP to DMD iPSC-CM cultures resulted in a similar reduction of the NADPH-dependent ROS production of NOX4.

Elevated ATP concentrations can be used by skeletal and cardiac myosin to increase cross-bridge binding and cycling, leading to stronger and faster contraction and relaxation (*55*). Cardiac-specific overexpression by means of recombinant adeno-associated viral (rAAV)-mediated delivery of the enzyme ribonucleotide reductase that converts adenosine diphosphate (ADP) to deoxy-ADP (dADP), which, on its turn, is rapidly converted to deoxy-ATP (dATP) in cells, facilitated CM contraction and cardiac performance in normal rodent hearts as well as in rodent and pig infarcted hearts (*56, 57*). We showed improved contractile properties of EHTs derived from DMD iPSC-CMs upon idebenone administration at physiological $Ca^{2+}$ concentrations. Preincubation of idebenone with PTC124 further enhanced the contractility, probably due to the PTC124-induced re-expression of Dystrophin proteins. In line with these results, the group of Olson performed CRISPR/Cas9-mediated exon skipping (“myoediting”) for DMD mutation corrections, in order to rescue the contractile dysfunction of DMD iPSC-CMs that were differentiated in 3D EHTs (*44, 45, 58*).

In conclusion, by using iPSC-CMs from DMD patients, we provided the first evidence that NOX4 expression and activity was significantly upregulated, contributing to high intracellular ROS and increased cell death. Furthermore, we compared the effects of the ROS

scavenger NAC, the read-through premature termination codon chemical drug PTC124 and idebenone in an *in vitro* setting of cardiomyopathic DMD. Finally, we gained novel mechanistic insights in the mode-of-action of idebenone on the hyperactive state of NOX4-mediated ROS production. Idebenone-mediated stimulation of the ATP production by the ETC of mitochondria could increase the affinity of ATP to bind with NOX4, reducing the ROS-producing activity of NOX4. Considering the early cellular stress responses present in iPSC-CMs from DMD patients, interfering with any of these early cellular events that lead to excessive ROS signals would positively affect the mitochondrial activity resulting in an improved contractile function.

# MATERIALS AND METHODS

*Study Design*

The objective of this study is to develop a stem cell-based model to investigate pathological mechanisms and evaluate their therapeutical potential in cardiomyopathy in DMD patients. The study was conducted in compliance with the principles of the Declaration of Helsinki, the principles of 'Good Clinical Practice' (GCP) and in accordance with all applicable regulatory requirements. The use of human samples from healthy control donors and DMD subjects for experimental purposes and protocols in the present study was approved by the Ethics Committee of the University Hospitals Leuven (respectively, S55438 and S65190). Subjects information, used in this study, is summarized in Table S1.

*Chemicals and Reagents*

NAC (Merck), ataluren (PTC124; Selleckchem) and idebenone (Santhera Pharmaceuticals, Pratteln Switzerland). Staurosporine (STS; Merck). CM-$H_2$DCFDA Total Intracellular ROS Indicator, JC-1 Mitochondrial Membrane Potential Probe, MitoSOX Red Mitochondrial Superoxide Indicator and MitoTracker-Red CMXRos Mitochondria Probe (all from Thermo Fisher Scientific). ATP Solution, Luminescent ATP Detection Assay Kit, Colorimetric NADPH Assay Kit (both from Abcam) and Mitochondrial Isolation Kit for Cultured Cells (Thermo Fisher Scientific).

*Generation of Integration-Free DMD iPSCs*

hFs and hPBMCs were isolated from DMD patients with known *Dystrophin* mutations (Table S1). Somatic cells were reprogrammed towards pluripotency using the integration-free SeV-based technology, performed according to the manufacturer's instructions (CytoTune-iPS 2.0 Sendai Reprogramming Kit; Thermo Fisher Scientific).

452

453 *Teratoma Formation Assay*

454 Pluripotency of SeV-reprogrammed iPSCs was evaluated *in vivo* in 6- to 8-week-old
455 immunodeficient *Rag2-null γc-null*/Balb/C mice. Teratoma formation experiments in mice
456 were conducted following the guidelines of the Animal Welfare Committee of Leuven
457 University and Belgian/European legislation (approved July 2016; P174/2016).

458

459 *Human iPSC Culture*

460 Human control and DMD diseased iPSC lines (Table S1) were cultured feeder-free on Geltrex
461 LDEV-Free hESC-Qualified Reduced Growth Factor Basement Membrane Matrix and
462 maintained in Essential 8 Flex Basal Medium supplemented with Essential 8 Flex Supplement
463 (50x) and 0.1% Pen/Strep (all from Thermo Fisher Scientific), at 37°C under normoxic
464 conditions (21% $O_2$ and 5% $CO_2$). Colonies were routinely passaged non-enzymatically with
465 0.5 mM EDTA in Phosphate-Buffered Saline (PBS; both from Thermo Fisher Scientific).
466 Mycoplasma contamination was assessed on a periodic basis for all cell cultures. No
467 contaminated cells were used in the described experiments of this study.

468

469 *Generation of DMD Isogenic Control Line through CRISPR/Cas9 Genome Editing*

470 To restore full-length expression of the *Dystrophin* gene, the isogenic control for the DMD
471 iPSC patient line, characterized by a genetic point mutation in exon 35 (c.4,996C > T;
472 p.Arg1,666X) of the *Dystrophin* gene, was generated through CRISPR/Cas9 from the *S.*
473 *pyogenes* system (5'-NGG PAM) as previously described (*59*). Briefly, two 20-nucleotide
474 sgRNAs (sgRNA #1: FW seq. CACCG-ATTTAACCACTCTTCTGCTC and RV seq. AAAC-
475 GAGCAGAAGAGTGGTTAAAT-C; sgRNA #2: FW seq. CACCG-
476 TAACCACTCTTCTGCTCAGG and RV seq. AAAC-CCTGAGCAGAAGAGTGGTTA-C)

were designed and ligated into the RNA-guided nuclease plasmid (pX330-mCherry plasmid; Addgene), in order to induce the Cas9-mediated DSB in the genomic DNA of the Dystrophin-deficient iPSCs. Cas9-mediated genome editing was performed via HDR. The targeted DNA modification required the use of a plasmid-based donor repair template with two homology arm regions for the *Dystrophin* gene, flanking a GFP-Hygromycin-TK expressing cassette for selection. Here, one of the homology arms contained the genetic correction of the nonsense mutation in the *Dystrophin* gene. Finally, a completely gene editing-free DMD isogenic iPSC line was obtained due to PiggyBac excision and FIAU selection, restoring the expression of functional Dystrophin protein (Table S1).

*Monolayer-Based Cardiac Differentiation of Human iPSCs*

Human iPSCs were differentiated into functional CMs according to a monolayer-based cardiac differentiation protocol, as previously described (*29*). Briefly, prior to differentiation, control and DMD iPSC lines were split in small colonies and subsequently cultured on a thin Matrigel Growth Factor Reduced (GFR) Basement Membrane Matrix layer (Corning) in complete Essential 8 Flex Medium at 37°C under hypoxic conditions (5% $O_2$ and 5% $CO_2$), in order to obtain the optimal confluency of 85%, three days after splitting. Mesoderm differentiation (day 0) was induced using 6 μM CHIR99021 (Axon Medchem) for 48 h in a chemically defined medium consisting of RPMI 1640 (Thermo Fisher Scientific), 500 μg/mL rice-derived recombinant human albumin and 213 μg/mL L-ascorbic acid 2-phosphate (both from Merck). After 24 h of CHIR99021 stimulation, iPSCs were transferred from hypoxia to normoxia. At day 2 of differentiation, iPSC-derived mesodermal cells were fed with basal medium supplemented with 4 μM IWR-1 (Merck) for 48 h, to induce cardiac progenitor cell differentiation. From day 4 onwards, medium was changed every other day with CM maintenance medium (RPMI 1640, rice-derived recombinant human albumin and L-ascorbic

acid 2-phosphate). Contracting CMs appeared at day 8 or 9 of cardiac differentiation. DMD iPSC-CMs were treated with 3 mM NAC and 0.5 μM idebenone from day 8 onwards, and 20 μg/mL ataluren (PTC124) was supplemented to the cardiac differentiation medium from day 4 onwards. In *NOX4* knockdown experiments, 250 nM of single-stranded antisense oligonucleotides for silencing *NOX4* mRNA, called Antisense LNA GapmeRs (Qiagen), were added to the cell cultures at day 8 of differentiation.

*Generation of 3D EHT Constructs*

3D EHT constructs were generated from 8- to 10-day-old iPSC-CMs, as previously described (*30*). CMs were dissociated with Collagenase A (1 U/mL; Merck) for 20 minutes at 37°C and transferred to custom-made 2% agarose (UltraPure; Thermo Fisher Scientific) casting molds in 24-well plate formats. The single-cell suspension was maintained in DMEM low glucose medium, containing 10% Fetal Bovine Serum (FBS), 1% heat-inactivated Horse Serum (HS), 1% Pen/Strep (all from Thermo Fisher Scientific) and 0.1% Rho-associated protein kinase (ROCK) inhibitor (Y-27632; VWR). Each EHT construct consisted of 1.0 $x10^6$ cells, supplemented with GFR Matrigel, 5.06% fibrinogen (human plasma; Merck), 3U/mL thrombin (Stago BNL) and 1.44% aprotinin (Merck). The casting was performed around two flexible polydimethylsiloxane (PDMS) microposts within the agarose molds. After 2 h of incubation, polymerization formed a fibrin block around the microposts, embedding the single-cell suspension. The fibrin block was removed from the casting molds and transferred to 24-well plates, containing EHT medium composed of DMEM low glucose, 10% heat-inactivated HS, 1% Pen/Strep, 0.1% aprotinin and 0.1% Human Insulin Solution (Merck). Medium was changed every other day with EHT medium.

*Quantitative Real-Time PCR Analysis*

Total RNA was extracted using the PureLink RNA Mini Kit and treated with the TURBO DNA-Free DNase Kit to assure highly pure RNA. 1 µg RNA was reverse transcribed into cDNA with SuperScript III Reverse Transcriptase First-Strand Synthesis SuperMix. Quantitative Real-Time PCR was performed with the Platinum SYBR Green qPCR SuperMix-UDG (all from Thermo Fisher Scientific). The oligonucleotide primer sequences (all from IDT) are listed in Table S2. A 10-fold dilution series ranging from $10^{-3}$ to $10^{-8}$ of 50 ng/µL human genomic DNA was used to evaluate the primer efficiency. Delta Ct (ΔCt) values were calculated by subtracting the Ct values from the genes of interest with the Ct values of the housekeeping genes (*GAPDH, HPRT* and *RPL13a*).

*Flow Cytometric Analysis*

Differentiated iPSC-CMs were dissociated using Collagenase A (1 U/mL) for 20 minutes at 37°C. All flow cytometry procedures were performed according to the manufacturer's instructions. Hank's Balanced Salt Solution (HBSS; pH 7.2) with $CaCl_2$ and $MgCl_2$ supplemented with 2% FBS (both from Thermo Fisher Scientific), 10 mM HEPES and 10 mM $NaN_3$ (both from Merck), was used as staining buffer. For high CM purity, iPSC-CMs were stained for the surface marker SIRPA (data not shown). If intracellular staining was necessary, cells were fixed with 4% paraformaldehyde (PFA; Polysciences) for 10 minutes at 37°C and permeabilized in ice-cold 90% methanol (Merck) for 30 minutes on ice, before the staining procedure. Fluorescence minus one (FMO) controls and compensations were included for appropriate gating. Samples were analyzed using the FACS Canto II HTS (BD Biosciences) and quantified using FlowJo Software Version 10 (FlowJo LLC). Table S3 provides a list of all flow cytometric antibodies used in this study.

552 *Immunofluorescence Imaging*

553 Cells were fixed with 4% PFA for 10 minutes at 4°C, permeabilized for 30 minutes at room
554 temperature in PBS supplemented with 0.2% Triton X-100 and 1% Bovine Serum Albumin
555 (BSA) and blocked for 30 minutes at room temperature in 10% donkey serum (all from Merck).
556 Samples were stained overnight at 4°C with the primary antibodies, followed by the appropriate
557 secondary antibodies (1 h incubation at room temperature). Immunofluorescent primary and
558 secondary antibodies were listed in Table S3. Nuclei were counterstained with 10 μg/mL
559 Hoechst (33342; Thermo Fisher Scientific). Analyses were assessed using the Nikon Eclipse Ti
560 Microscope or the Nikon Eclipse Ti A1R Configurated Confocal Microscope, with appropriate
561 NIS-Elements Software (all from Nikon).

562

563 *Mitochondria and Cytoplasmic Fractionation*

564 Mitochondrial and cytoplasmic separation was performed using the Mitochondrial Isolation Kit
565 for Cultured Cells (Thermo Fisher Scientific), according to the manufacturer's instructions with
566 minor modifications. To obtain a more purified mitochondrial fraction (with a more than 50%
567 reduction of the lysosomal and peroxisomal contaminants), the post-cell debris supernatant was
568 subjected to an extra centrifuge step at 3000 x g for 15 minutes. For Western blot analysis,
569 mitochondrial pellets were lysed with 2% CHAPS (Merck) in Tris-buffered saline (TBS;
570 containing 25 mM Tris, 0.15 M NaCl; pH 7.2) and subsequently centrifuged at high speed for
571 2 minutes. Western blot analysis was performed on the supernatant, containing soluble
572 mitochondrial protein.

573

574 *Western Blot Analysis*

575 Western blot analysis for cell lysates was performed in RIPA buffer supplemented with 10 mM
576 NaF, 0.5 mM $Na_3VO_4$, 1:100 protease inhibitor cocktail and 1 mM Phenylmethylsulfonyl

Fluoride (PMSF; all from Merck). Equal amounts of protein (40 µg) were heat-denaturated at 95°C in sample-loading buffer (50 mM Tris-HCl, 100 mM DTT, 2% SDS, 0.1% bromophenol blue and 10% glycerol; pH 6.8), resolved by SDS-polyacrylamide gel electrophoresis and subsequently transferred to nitrocellulose membranes (Amersham Protran Western Blotting Membranes; Merck). The filters were blocked with TBS containing 0.05% Tween and 5% non-fat dry milk (Merck). Incubation was done overnight with the indicated primary antibody dilutions, as listed in Table S2. Horseradish peroxidase-conjugated secondary antibodies (Bio-Rad) were diluted 1:5,000 in TBS-Tween (0.05%) with 2.5% non-fat dry milk. After incubation with SuperSignal Pico or Femto chemiluminescence substrate (both from Thermo Fisher Scientific), the polypeptide bands were detected with GelDoc Chemiluminescence Detection System (Bio-Rad). Quantification of relative densitometry was obtained by normalizing to the background and to loading control proteins (ACTB, from Cell Signaling Technology) using Image Lab Software (Bio-Rad).

*Patch-Clamp Electrophysiology and $Ca^{2+}$ Recordings*

Single cells were seeded on Matrigel-coated coverslips. Cells were perfused at 37°C with a solution containing the following (in mM): 137 NaCl, 5.4 KCl, 1.8 $CaCl_2$, 0.5 $MgCl_2$, 10 glucose and 10 Na-HEPES. The pH was adjusted to 7.4 with NaOH. The patch-clamp pipettes were filled with a solution containing the following (in mM): 120 K-Asp, 20 KCl, 10 HEPES, 5 Mg-ATP, 10 NaCl and 0.05 $K_5$Fluo-4. The pH was adjusted to 7.2 with KOH. Patch electrode resistances were between 2.5 and 3 MΩ when the pipettes were filled with intracellular solution. Cells were patched in the whole-cell configuration. Data were recorded using an Axopatch 200B amplifier (Axon Instruments) at a sampling rate of 10 kHz. Signals were filtered with 5 kHz low-pass Bessel filters. Action potentials (APs) were recorded in current-clamp mode, and if not spontaneous, after a 5 ms pulse of 0.5 nA at a 1 Hz frequency. $Ca^{2+}$ currents were

602 measured in voltage-clamp mode. After a $Na^+$ current inactivation step from -70 mV to 40 mV
603 for 750 ms, $Ca^{2+}$ currents were recorded with 10 mV voltage steps from -40 mV to 60 mV
604 during 205 ms. For analysis, the maximum amplitude of the $Ca^{2+}$ current was measured and
605 corrected for the cell capacitance. Data were analyzed with Clampfit Software (Axon
606 Instruments).
607
608 *Contractility Measurements of 3D EHT Constructs*
609 The contractile properties of 3D EHTs were monitored by measuring the deflection distances
610 of the microposts of the EHT device (in μm) during spontaneous contraction and relaxation
611 under temperature-controlled conditions (37°C) in oxygenated Tyrode's solution (in mM;
612 containing 137 NaCl, 5.4 KCl, 0.5 $MgCl_2$, 12.8 HEPES and 5.5 Glucose; dissolved in deionized
613 sterile water at pH 7.4) with $Ca^{2+}$. A $Ca^{2+}$ concentration of 1.8 mM was used to mimic
614 physiological conditions. EHT constructs for contractility measurements were generated from
615 8-day-old iPSC-CMs and monitored after 5 days of EHT maturation.
616
617 *ATP Luminescence and NADPH Detection*
618 The level of ATP was measured using the Luminescent ATP Detection Assay Kit (Abcam),
619 according to the manufacturer's instructions. Recordings were performed with the EG&G
620 Berthold Microplate Luminometer LB 96V and corresponding software (Berthold
621 Technologies). Using the NADPH Assay Kit (Abcam), NADPH-dependent ROS production
622 was measured in the presence or absence of 2.5 or 5.0 mM ATP (preincubated for 60 minutes)
623 in the total CM fraction or isolated mitochondrial fraction, according to the manufacturer's
624 instructions. Recordings were performed with the ELx808 Absorbance Microplate Reader and
625 quantified using Gen5 Software Version 3 (both from BioTek Instruments).
626

627 *Statistical Analysis*

628 Data were statistically analyzed using Prism Software Version 8 (GraphPad). All data were
629 reported as mean ± standard error of the mean (SEM). Differences between two groups were
630 examined for statistical significance using Student's t-test. One-Way or Two-Way ANOVA
631 (with multiple comparisons test and Tukey's or Bonferroni's correction) were used for three or
632 more groups. Significance of the difference was indicated as follows: *P < 0.05; **P < 0.01;
633 ***P < 0.001 and ****P < 0.0001.

# REFERENCES


1. T. S. Li, M. Takahashi, R. Suzuki, T. Kobayashi, H. Ito, A. Mikamo, K. Hamano, Pravastatin improves remodeling and cardiac function after myocardial infarction by an antiinflammatory mechanism rather than by the induction of angiogenesis. *Ann Thorac Surg* **81**, 2217-2225 (2006).
2. C. L. Mummery, J. Zhang, E. S. Ng, D. A. Elliott, A. G. Elefanty, T. J. Kamp, Differentiation of human embryonic stem cells and induced pluripotent stem cells to cardiomyocytes: a methods overview. *Circ Res* **111**, 344-358 (2012).
3. E. Mercuri, C. G. Bonnemann, F. Muntoni, Muscular dystrophies. *Lancet* **394**, 2025-2038 (2019).
4. A. E. Emery, The muscular dystrophies. *Lancet* **359**, 687-695 (2002).
5. E. Landfeldt, R. Thompson, T. Sejersen, H. J. McMillan, J. Kirschner, H. Lochmuller, Life expectancy at birth in Duchenne muscular dystrophy: a systematic review and meta-analysis. *Eur J Epidemiol* **35**, 643-653 (2020).
6. K. E. Davies, K. J. Nowak, Molecular mechanisms of muscular dystrophies: old and new players. *Nat Rev Mol Cell Biol* **7**, 762-773 (2006).
7. D. G. Allen, N. P. Whitehead, S. C. Froehner, Absence of Dystrophin Disrupts Skeletal Muscle Signaling: Roles of Ca2+, Reactive Oxygen Species, and Nitric Oxide in the Development of Muscular Dystrophy. *Physiol Rev* **96**, 253-305 (2016).
8. H. D. Sesso, J. E. Buring, W. G. Christen, T. Kurth, C. Belanger, J. MacFadyen, V. Bubes, J. E. Manson, R. J. Glynn, J. M. Gaziano, Vitamins E and C in the prevention of cardiovascular disease in men: the Physicians' Health Study II randomized controlled trial. *JAMA* **300**, 2123-2133 (2008).

9. I. Heart Outcomes Prevention Evaluation Study, S. Yusuf, G. Dagenais, J. Pogue, J. Bosch, P. Sleight, Vitamin E supplementation and cardiovascular events in high-risk patients. *N Engl J Med* **342**, 154-160 (2000).

10. K. Bedard, K. H. Krause, The NOX family of ROS-generating NADPH oxidases: physiology and pathophysiology. *Physiol Rev* **87**, 245-313 (2007).

11. A. Vermot, I. Petit-Hartlein, S. M. E. Smith, F. Fieschi, NADPH Oxidases (NOX): An Overview from Discovery, Molecular Mechanisms to Physiology and Pathology. *Antioxidants (Basel)* **10**, (2021).

12. T. Ago, J. Kuroda, J. Pain, C. Fu, H. Li, J. Sadoshima, Upregulation of Nox4 by hypertrophic stimuli promotes apoptosis and mitochondrial dysfunction in cardiac myocytes. *Circ Res* **106**, 1253-1264 (2010).

13. J. Kuroda, T. Ago, S. Matsushima, P. Zhai, M. D. Schneider, J. Sadoshima, NADPH oxidase 4 (Nox4) is a major source of oxidative stress in the failing heart. *Proc Natl Acad Sci U S A* **107**, 15565-15570 (2010).

14. C. F. Spurney, S. Knoblach, E. E. Pistilli, K. Nagaraju, G. R. Martin, E. P. Hoffman, Dystrophin-deficient cardiomyopathy in mouse: expression of Nox4 and Lox are associated with fibrosis and altered functional parameters in the heart. *Neuromuscul Disord* **18**, 371-381 (2008).

15. Z. V. Varga, M. Pipicz, J. A. Baan, T. Baranyai, G. Koncsos, P. Leszek, M. Kusmierczyk, F. Sanchez-Cabo, P. Garcia-Pavia, G. J. Brenner, Z. Giricz, T. Csont, L. Mendler, E. Lara-Pezzi, P. Pacher, P. Ferdinandy, Alternative Splicing of NOX4 in the Failing Human Heart. *Front Physiol* **8**, 935 (2017).

16. M. Zhang, A. Perino, A. Ghigo, E. Hirsch, A. M. Shah, NADPH oxidases in heart failure: poachers or gamekeepers? *Antioxid Redox Signal* **18**, 1024-1041 (2013).

17. K. D. Martyn, L. M. Frederick, K. von Loehneysen, M. C. Dinauer, U. G. Knaus, Functional analysis of Nox4 reveals unique characteristics compared to other NADPH oxidases. *Cell Signal* **18**, 69-82 (2006).

18. M. Zhang, A. C. Brewer, K. Schroder, C. X. Santos, D. J. Grieve, M. Wang, N. Anilkumar, B. Yu, X. Dong, S. J. Walker, R. P. Brandes, A. M. Shah, NADPH oxidase-4 mediates protection against chronic load-induced stress in mouse hearts by enhancing angiogenesis. *Proc Natl Acad Sci U S A* **107**, 18121-18126 (2010).

19. R. J. Khairallah, G. Shi, F. Sbrana, B. L. Prosser, C. Borroto, M. J. Mazaitis, E. P. Hoffman, A. Mahurkar, F. Sachs, Y. Sun, Y. W. Chen, R. Raiteri, W. J. Lederer, S. G. Dorsey, C. W. Ward, Microtubules underlie dysfunction in duchenne muscular dystrophy. *Sci Signal* **5**, ra56 (2012).

20. B. Wu, H. M. Moulton, P. L. Iversen, J. Jiang, J. Li, J. Li, C. F. Spurney, A. Sali, A. D. Guerron, K. Nagaraju, T. Doran, P. Lu, X. Xiao, Q. L. Lu, Effective rescue of dystrophin improves cardiac function in dystrophin-deficient mice by a modified morpholino oligomer. *Proc Natl Acad Sci U S A* **105**, 14814-14819 (2008).

21. E. M. Welch, E. R. Barton, J. Zhuo, Y. Tomizawa, W. J. Friesen, P. Trifillis, S. Paushkin, M. Patel, C. R. Trotta, S. Hwang, R. G. Wilde, G. Karp, J. Takasugi, G. Chen, S. Jones, H. Ren, Y. C. Moon, D. Corson, A. A. Turpoff, J. A. Campbell, M. M. Conn, A. Khan, N. G. Almstead, J. Hedrick, A. Mollin, N. Risher, M. Weetall, S. Yeh, A. A. Branstrom, J. M. Colacino, J. Babiak, W. D. Ju, S. Hirawat, V. J. Northcutt, L. L. Miller, P. Spatrick, F. He, M. Kawana, H. Feng, A. Jacobson, S. W. Peltz, H. L. Sweeney, PTC124 targets genetic disorders caused by nonsense mutations. *Nature* **447**, 87-91 (2007).

22. A. Moretti, L. Fonteyne, F. Giesert, P. Hoppmann, A. B. Meier, T. Bozoglu, A. Baehr, C. M. Schneider, D. Sinnecker, K. Klett, T. Frohlich, F. A. Rahman, T. Haufe, S. Sun,

V. Jurisch, B. Kessler, R. Hinkel, R. Dirschinger, E. Martens, C. Jilek, A. Graf, S. Krebs, G. Santamaria, M. Kurome, V. Zakhartchenko, B. Campbell, K. Voelse, A. Wolf, T. Ziegler, S. Reichert, S. Lee, F. Flenkenthaler, T. Dorn, I. Jeremias, H. Blum, A. Dendorfer, A. Schnieke, S. Krause, M. C. Walter, N. Klymiuk, K. L. Laugwitz, E. Wolf, W. Wurst, C. Kupatt, Somatic gene editing ameliorates skeletal and cardiac muscle failure in pig and human models of Duchenne muscular dystrophy. *Nat Med* **26**, 207-214 (2020).

23. A. Bajek, D. Porowinska, T. Kloskowski, E. Brzoska, M. A. Ciemerych, T. Drewa, Cell therapy in Duchenne muscular dystrophy treatment: clinical trials overview. *Crit Rev Eukaryot Gene Expr* **25**, 1-11 (2015).

24. M. P. Calos, The CRISPR Way to Think about Duchenne's. *N Engl J Med* **374**, 1684-1686 (2016).

25. C. S. Young, M. R. Hicks, N. V. Ermolova, H. Nakano, M. Jan, S. Younesi, S. Karumbayaram, C. Kumagai-Cresse, D. Wang, J. A. Zack, D. B. Kohn, A. Nakano, S. F. Nelson, M. C. Miceli, M. J. Spencer, A. D. Pyle, A Single CRISPR-Cas9 Deletion Strategy that Targets the Majority of DMD Patients Restores Dystrophin Function in hiPSC-Derived Muscle Cells. *Cell Stem Cell* **18**, 533-540 (2016).

26. I. E. C. Verhaart, A. Aartsma-Rus, Therapeutic developments for Duchenne muscular dystrophy. *Nat Rev Neurol* **15**, 373-386 (2019).

27. G. M. Buyse, N. Goemans, M. van den Hauwe, D. Thijs, I. J. de Groot, U. Schara, B. Ceulemans, T. Meier, L. Mertens, Idebenone as a novel, therapeutic approach for Duchenne muscular dystrophy: results from a 12 month, double-blind, randomized placebo-controlled trial. *Neuromuscul Disord* **21**, 396-405 (2011).

28. G. M. Buyse, T. Voit, U. Schara, C. S. M. Straathof, M. G. D'Angelo, G. Bernert, J. M. Cuisset, R. S. Finkel, N. Goemans, C. M. McDonald, C. Rummey, T. Meier, D. S.

Group, Efficacy of idebenone on respiratory function in patients with Duchenne muscular dystrophy not using glucocorticoids (DELOS): a double-blind randomised placebo-controlled phase 3 trial. *Lancet* **385**, 1748-1757 (2015).

29. P. W. Burridge, E. Matsa, P. Shukla, Z. C. Lin, J. M. Churko, A. D. Ebert, F. Lan, S. Diecke, B. Huber, N. M. Mordwinkin, J. R. Plews, O. J. Abilez, B. Cui, J. D. Gold, J. C. Wu, Chemically defined generation of human cardiomyocytes. *Nat Methods* **11**, 855-860 (2014).

30. K. Breckwoldt, D. Letuffe-Breniere, I. Mannhardt, T. Schulze, B. Ulmer, T. Werner, A. Benzin, B. Klampe, M. C. Reinsch, S. Laufer, A. Shibamiya, M. Prondzynski, G. Mearini, D. Schade, S. Fuchs, C. Neuber, E. Kramer, U. Saleem, M. L. Schulze, M. L. Rodriguez, T. Eschenhagen, A. Hansen, Differentiation of cardiomyocytes and generation of human engineered heart tissue. *Nat Protoc* **12**, 1177-1197 (2017).

31. B. Eisen, R. Ben Jehuda, A. J. Cuttitta, L. N. Mekies, Y. Shemer, P. Baskin, I. Reiter, L. Willi, D. Freimark, M. Gherghiceanu, L. Monserrat, M. Scherr, D. Hilfiker-Kleiner, M. Arad, D. E. Michele, O. Binah, Electrophysiological abnormalities in induced pluripotent stem cell-derived cardiomyocytes generated from Duchenne muscular dystrophy patients. *J Cell Mol Med* **23**, 2125-2135 (2019).

32. B. Lin, Y. Li, L. Han, A. D. Kaplan, Y. Ao, S. Kalra, G. C. Bett, R. L. Rasmusson, C. Denning, L. Yang, Modeling and study of the mechanism of dilated cardiomyopathy using induced pluripotent stem cells derived from individuals with Duchenne muscular dystrophy. *Dis Model Mech* **8**, 457-466 (2015).

33. X. Guan, D. L. Mack, C. M. Moreno, J. L. Strande, J. Mathieu, Y. Shi, C. D. Markert, Z. Wang, G. Liu, M. W. Lawlor, E. C. Moorefield, T. N. Jones, J. A. Fugate, M. E. Furth, C. E. Murry, H. Ruohola-Baker, Y. Zhang, L. F. Santana, M. K. Childers,

Dystrophin-deficient cardiomyocytes derived from human urine: new biologic reagents for drug discovery. *Stem Cell Res* **12**, 467-480 (2014).

34. F. Tsurumi, S. Baba, D. Yoshinaga, K. Umeda, T. Hirata, J. Takita, T. Heike, The intracellular Ca2+ concentration is elevated in cardiomyocytes differentiated from hiPSCs derived from a Duchenne muscular dystrophy patient. *PLoS One* **14**, e0213768 (2019).

35. M. Sato, N. Shiba, D. Miyazaki, Y. Shiba, Y. Echigoya, T. Yokota, H. Takizawa, Y. Aoki, S. Takeda, A. Nakamura, Amelioration of intracellular Ca(2+) regulation by exon-45 skipping in Duchenne muscular dystrophy-induced pluripotent stem cell-derived cardiomyocytes. *Biochem Biophys Res Commun* **520**, 179-185 (2019).

36. J. M. Pioner, X. Guan, J. M. Klaiman, A. W. Racca, L. Pabon, V. Muskheli, J. Macadangdang, C. Ferrantini, M. R. Hoopmann, R. L. Moritz, D. H. Kim, C. Tesi, C. Poggesi, C. E. Murry, M. K. Childers, D. L. Mack, M. Regnier, Absence of full-length dystrophin impairs normal maturation and contraction of cardiomyocytes derived from human-induced pluripotent stem cells. *Cardiovasc Res* **116**, 368-382 (2020).

37. C. Jung, A. S. Martins, E. Niggli, N. Shirokova, Dystrophic cardiomyopathy: amplification of cellular damage by Ca2+ signalling and reactive oxygen species-generating pathways. *Cardiovasc Res* **77**, 766-773 (2008).

38. C. A. Timpani, A. Hayes, E. Rybalka, Revisiting the dystrophin-ATP connection: How half a century of research still implicates mitochondrial dysfunction in Duchenne Muscular Dystrophy aetiology. *Med Hypotheses* **85**, 1021-1033 (2015).

39. L. D. Zorova, V. A. Popkov, E. Y. Plotnikov, D. N. Silachev, I. B. Pevzner, S. S. Jankauskas, V. A. Babenko, S. D. Zorov, A. V. Balakireva, M. Juhaszova, S. J. Sollott, D. B. Zorov, Mitochondrial membrane potential. *Anal Biochem* **552**, 50-59 (2018).

40. A. Mathur, Y. Hong, B. K. Kemp, A. A. Barrientos, J. D. Erusalimsky, Evaluation of fluorescent dyes for the detection of mitochondrial membrane potential changes in cultured cardiomyocytes. *Cardiovasc Res* **46**, 126-138 (2000).

41. C. A. Belmokhtar, J. Hillion, E. Segal-Bendirdjian, Staurosporine induces apoptosis through both caspase-dependent and caspase-independent mechanisms. *Oncogene* **20**, 3354-3362 (2001).

42. K. Block, Y. Gorin, H. E. Abboud, Subcellular localization of Nox4 and regulation in diabetes. *Proc Natl Acad Sci U S A* **106**, 14385-14390 (2009).

43. K. Shanmugasundaram, B. K. Nayak, W. E. Friedrichs, D. Kaushik, R. Rodriguez, K. Block, NOX4 functions as a mitochondrial energetic sensor coupling cancer metabolic reprogramming to drug resistance. *Nat Commun* **8**, 997 (2017).

44. V. Kyrychenko, S. Kyrychenko, M. Tiburcy, J. M. Shelton, C. Long, J. W. Schneider, W. H. Zimmermann, R. Bassel-Duby, E. N. Olson, Functional correction of dystrophin actin binding domain mutations by genome editing. *JCI Insight* **2**, (2017).

45. C. Long, H. Li, M. Tiburcy, C. Rodriguez-Caycedo, V. Kyrychenko, H. Zhou, Y. Zhang, Y. L. Min, J. M. Shelton, P. P. A. Mammen, N. Y. Liaw, W. H. Zimmermann, R. Bassel-Duby, J. W. Schneider, E. N. Olson, Correction of diverse muscular dystrophy mutations in human engineered heart muscle by single-site genome editing. *Sci Adv* **4**, eaap9004 (2018).

46. N. Cao, Z. Liu, Z. Chen, J. Wang, T. Chen, X. Zhao, Y. Ma, L. Qin, J. Kang, B. Wei, L. Wang, Y. Jin, H. T. Yang, Ascorbic acid enhances the cardiac differentiation of induced pluripotent stem cells through promoting the proliferation of cardiac progenitor cells. *Cell Res* **22**, 219-236 (2012).

47. H. Fukumura, M. Sato, K. Kezuka, I. Sato, X. Feng, S. Okumura, T. Fujita, U. Yokoyama, H. Eguchi, Y. Ishikawa, T. Saito, Effect of ascorbic acid on reactive oxygen

804 species production in chemotherapy and hyperthermia in prostate cancer cells. *J Physiol*
805 *Sci* **62**, 251-257 (2012).
806 48. X. Wei, Y. Xu, F. F. Xu, L. Chaiswing, D. Schnell, T. Noel, C. Wang, J. Chen, D. K. St
807 Clair, W. H. St Clair, RelB Expression Determines the Differential Effects of Ascorbic
808 Acid in Normal and Cancer Cells. *Cancer Res* **77**, 1345-1356 (2017).
809 49. C. Bartsch, M. M. Bekhite, A. Wolheim, M. Richter, C. Ruhe, B. Wissuwa, A.
810 Marciniak, J. Muller, R. Heller, H. R. Figulla, H. Sauer, M. Wartenberg, NADPH
811 oxidase and eNOS control cardiomyogenesis in mouse embryonic stem cells on ascorbic
812 acid treatment. *Free Radic Biol Med* **51**, 432-443 (2011).
813 50. H. Yasutake, J. K. Lee, A. Hashimoto, K. Masuyama, J. Li, Y. Kuramoto, S. Higo, S.
814 Hikoso, K. Hidaka, A. T. Naito, S. Miyagawa, Y. Sawa, I. Komuro, Y. Sakata,
815 Decreased YAP activity reduces proliferative ability in human induced pluripotent stem
816 cell of duchenne muscular dystrophy derived cardiomyocytes. *Sci Rep* **11**, 10351
817 (2021).
818 51. B. L. Prosser, C. W. Ward, W. J. Lederer, X-ROS signaling: rapid mechano-chemo
819 transduction in heart. *Science* **333**, 1440-1445 (2011).
820 52. J. P. Kerr, P. Robison, G. Shi, A. I. Bogush, A. M. Kempema, J. K. Hexum, N. Becerra,
821 D. A. Harki, S. S. Martin, R. Raiteri, B. L. Prosser, C. W. Ward, Detyrosinated
822 microtubules modulate mechanotransduction in heart and skeletal muscle. *Nat Commun*
823 **6**, 8526 (2015).
824 53. C. Campbell, R. J. Barohn, E. Bertini, B. Chabrol, G. P. Comi, B. T. Darras, R. S. Finkel,
825 K. M. Flanigan, N. Goemans, S. T. Iannaccone, K. J. Jones, J. Kirschner, J. K. Mah, K.
826 D. Mathews, C. M. McDonald, E. Mercuri, Y. Nevo, Y. Pereon, J. B. Renfroe, M. M.
827 Ryan, J. B. Sampson, U. Schara, T. Sejersen, K. Selby, M. Tulinius, J. J. Vilchez, T.
828 Voit, L. J. Wei, B. L. Wong, G. Elfring, M. Souza, J. McIntosh, P. Trifillis, S. W. Peltz,

F. Muntoni, P. G.-D. S. Group, A. D. S. Group, G. Clinical Evaluator Training, Meta-analyses of ataluren randomized controlled trials in nonsense mutation Duchenne muscular dystrophy. *J Comp Eff Res*, (2020).

54. J. E. Walker, M. Saraste, M. J. Runswick, N. J. Gay, Distantly related sequences in the alpha- and beta-subunits of ATP synthase, myosin, kinases and other ATP-requiring enzymes and a common nucleotide binding fold. *EMBO J* **1**, 945-951 (1982).

55. F. Moussavi-Harami, M. V. Razumova, A. W. Racca, Y. Cheng, A. Stempien-Otero, M. Regnier, 2-Deoxy adenosine triphosphate improves contraction in human end-stage heart failure. *J Mol Cell Cardiol* **79**, 256-263 (2015).

56. S. C. Kolwicz, Jr., G. L. Odom, S. G. Nowakowski, F. Moussavi-Harami, X. Chen, H. Reinecke, S. D. Hauschka, C. E. Murry, G. G. Mahairas, M. Regnier, AAV6-mediated Cardiac-specific Overexpression of Ribonucleotide Reductase Enhances Myocardial Contractility. *Mol Ther* **24**, 240-250 (2016).

57. S. Kadota, J. Carey, H. Reinecke, J. Leggett, S. Teichman, M. A. Laflamme, C. E. Murry, M. Regnier, G. G. Mahairas, Ribonucleotide reductase-mediated increase in dATP improves cardiac performance via myosin activation in a large animal model of heart failure. *Eur J Heart Fail* **17**, 772-781 (2015).

58. A. Atmanli, A. C. Chai, M. Cui, Z. Wang, T. Nishiyama, R. Bassel-Duby, E. N. Olson, Cardiac Myoediting Attenuates Cardiac Abnormalities in Human and Mouse Models of Duchenne Muscular Dystrophy. *Circ Res*, (2021).

59. F. A. Ran, P. D. Hsu, J. Wright, V. Agarwala, D. A. Scott, F. Zhang, Genome engineering using the CRISPR-Cas9 system. *Nat Protoc* **8**, 2281-2308 (2013).

60. A. M. Patel, K. Wierda, L. Thorrez, M. van Putten, J. De Smedt, L. Ribeiro, T. Tricot, M. Gajjar, R. Duelen, P. Van Damme, L. De Waele, N. Goemans, C. Tanganyika-de Winter, D. Costamagna, A. Aartsma-Rus, H. van Duyvenvoorde, M. Sampaolesi, G. M.

854 Buyse, C. M. Verfaillie, Dystrophin deficiency leads to dysfunctional glutamate
855 clearance in iPSC derived astrocytes. *Transl Psychiatry* **9**, 200 (2019).
856 61. M. Coll, L. Perea, R. Boon, S. B. Leite, J. Vallverdu, I. Mannaerts, A. Smout, A. El
857 Taghdouini, D. Blaya, D. Rodrigo-Torres, I. Graupera, B. Aguilar-Bravo, C. Chesne,
858 M. Najimi, E. Sokal, J. J. Lozano, L. A. van Grunsven, C. M. Verfaillie, P. Sancho-Bru,
859 Generation of Hepatic Stellate Cells from Human Pluripotent Stem Cells Enables In
860 Vitro Modeling of Liver Fibrosis. *Cell Stem Cell* **23**, 101-113 e107 (2018).
861 62. C. Rauch, E. Feifel, G. Kern, C. Murphy, F. Meier, W. Parson, M. Beilmann, P.
862 Jennings, G. Gstraunthaler, A. Wilmes, Differentiation of human iPSCs into functional
863 podocytes. *PLoS One* **13**, e0203869 (2018).

## ACKNOWLEDGEMENTS

The authors thank Santhera Pharmaceuticals (Pratteln, Switzerland) for providing idebenone. The authors gratefully acknowledge Hanne Grosemans and Sylvia Sauvage for technical assistance; Ewa Berlińska, Filippo Conti, Vittoria Marini and Ilaria Tortorella for the assistance during their internship period at the KU Leuven; and Christina Vochten and Vicky Raets for the administrative assistance. **Funding:** R.D. is supported by KU Leuven Rondoufonds voor Duchenne Onderzoek (EQQ-FODUCH-O2010), FWO (#G066821N) and the internal KU Leuven grant (C24/18/103). This work has been supported with the contribution of "Opening The Future" Campaign (EJJ-OPTFUT-02010), CARIPLO 2015_0634, FWO (#G0D4517N), GOA (EJJ-C2161-GOA/11/012), IUAP-VII/07 (EJJ-C4851-17/07-P), OT#09-053 (EJJ-C0420-OT/09/053) and KU Leuven C1-3DMuSyC (C14/17/111) grants. G.M.B. is Senior Clinical Investigator of the Research Foundation Flanders (FWO Vlaanderen, Belgium).

**Author contributions:** R.D. participated in conception and design, collection and assembly of data, data analysis and interpretation, and manuscript writing. D.C. participated in western blot collection and assembly of data, data analysis and interpretation, and reviewed the manuscript. G.G. participated in patch-clamp electrophysiology and $Ca^{2+}$ recordings, data analysis and interpretation, and reviewed the manuscript. L.D.W. provided DMD patient study samples, participated in conception and design, data analysis and interpretation, and reviewed the manuscript. N.G. provided DMD patient study samples, and reviewed the manuscript. K.D. participated in data analysis and interpretation, and reviewed the manuscript. C.M.V. participated in conception and design, data analysis and interpretation, and reviewed the manuscript. K.R.S. participated in conception and design, data analysis and interpretation, and reviewed the manuscript. G.M.B. and M.S. participated in conception and design, data analysis and interpretation, reviewed the manuscript, and gave final approval for manuscript submission.

**Competing interests:** G.M.B. was Investigator for clinical trials in DMD sponsored by

889 Santhera Pharmaceuticals. G.M.B. is co-inventor of relevant patent applications. The
890 investigators and authors had sole discretion over study design, collection, analysis and
891 interpretation of data, writing of the report and decision to submit the manuscript for
892 publication. All the other authors declare no competing interests. **Data and materials**
893 **availability:** All data generated or analyzed during this study are included in this published
894 article (and its supplementary information files).

# LIST OF FIGURES AND SUPPLEMENTARY MATERIALS



## Supplementary Materials:

**Fig. S4.** Lack of Dystrophin protein in iPSC-CMs from DMD patients resulted in premature cell death.

**Fig. S5.** Dystrophin re-expression in DMD iPSC-CMs after PTC124 treatment.

**Fig. S6.** Corresponding flow cytometric graphs and quantification for the characterization of the cardiomyopathic phenotype of DMD iPSC-CMs, showing premature cell death, depolarized mitochondria and increased intracellular ROS levels.

**Fig. S7.** Drug specificity on cell death and intracellular ROS concentrations in the experimental iPSC-CM groups.

**Fig. S8.** Drug specificity on $\Delta\Psi_m$ and mitochondrial superoxide concentrations in the experimental iPSC-CM groups.

**Fig. S9.** The specificity of the treatment options on the expression levels of NOX4 in iPSC-CM cultures.

**Fig. S10.** NOX4 protein expression levels after STS-induced cell death in DMD and control iPSC-CMs.

**Fig. S11.** Characterization of DMD patient-specific iPSC-CMs *in vitro*, showing increased NOX4 gene and protein expression levels, depolarized mitochondria and increased intracellular ROS levels.

**Fig. S12.** NADPH-dependent ROS production and intracellular ATP levels in DMD iPSC-CMs after idebenone application.

**Fig. S13.** The specificity of idebenone on the NADPH-dependent ROS production and ATP levels in the experimental iPSC-CM groups.

# FIGURES AND FIGURE LEGENDS

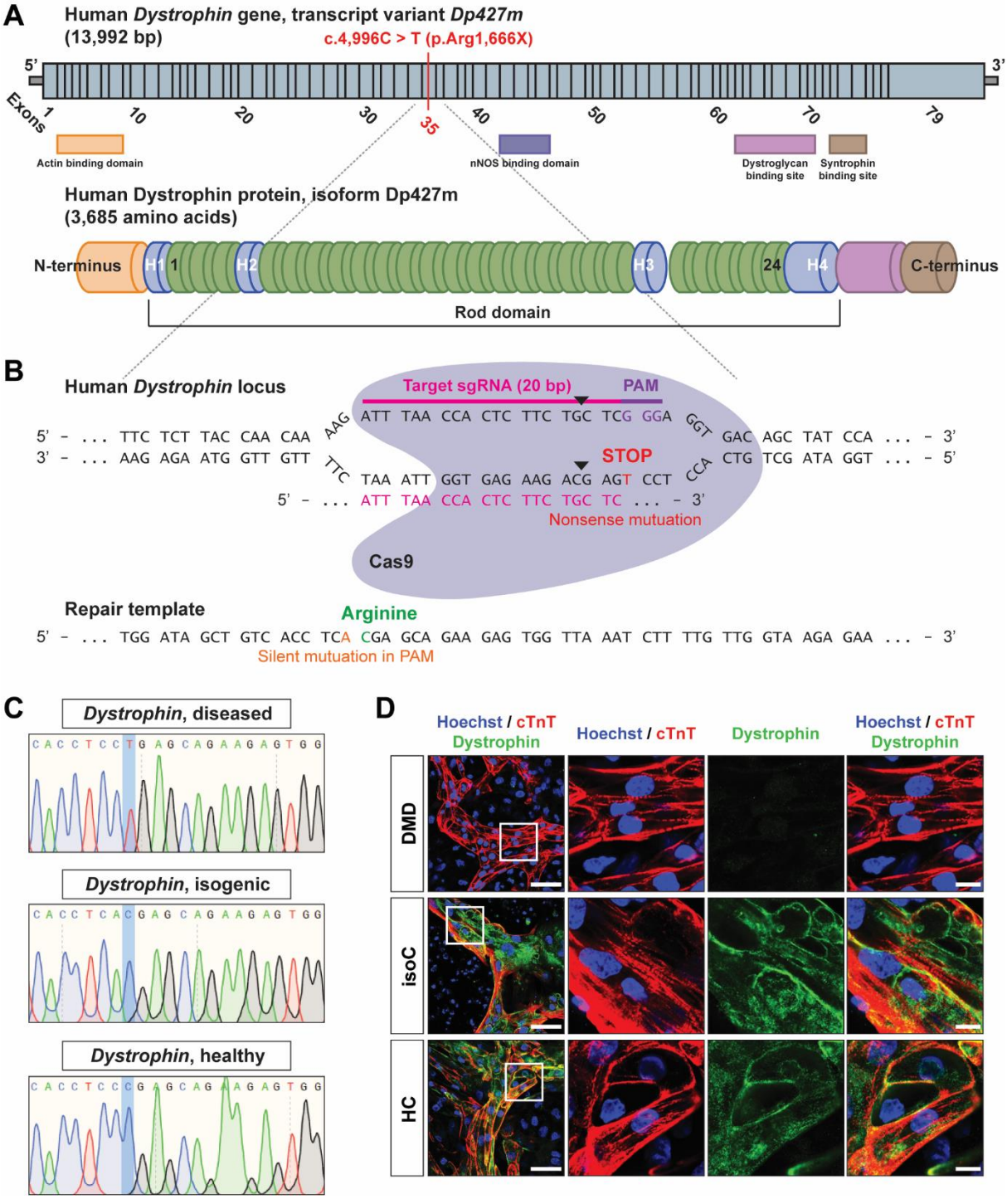


**Fig. 1: DMD iPSC CRISPR/Cas9 gene editing of a nonsense mutation in exon 35 (c.4,996C > T; p.Arg1,666X) of the *Dystrophin* gene. (A)** Schematic representation of the human *Dystrophin* gene sequence (*top*, transcript variant *Dp427m*) and the encoded Dystrophin protein (*bottom*, isoform Dp427m). The genetic point mutation is located in exon 35 of the *Dystrophin*

947 gene, resulting in a premature stop codon. **(B)** The 20-nucleotide sgRNA
948 (ATTTAACCACTCTTCTGCTC) to induce the Cas9-mediated DSB (indicated as black
949 triangles). The donor repair template, containing the CRISPR/Cas9-mediated genetic correction
950 of the nonsense mutation in the *Dystrophin* gene. **(C)** DNA sequencing of the mutated region
951 of interest of the *Dystrophin* gene before (DMD diseased) and after (DMD isogenic)
952 CRISPR/Cas9 gene editing. **(D)** Immunofluorescent staining showing the expression of
953 Dystrophin protein levels (green) in differentiated DMD iPSC-CMs (cTnT, red and Hoechst,
954 blue) after CRISPR/Cas9-mediated genetic correction. Scale bar: 50 μm. White boxes with
955 corresponding insets at higher magnification. Scale bar: 10 μm.

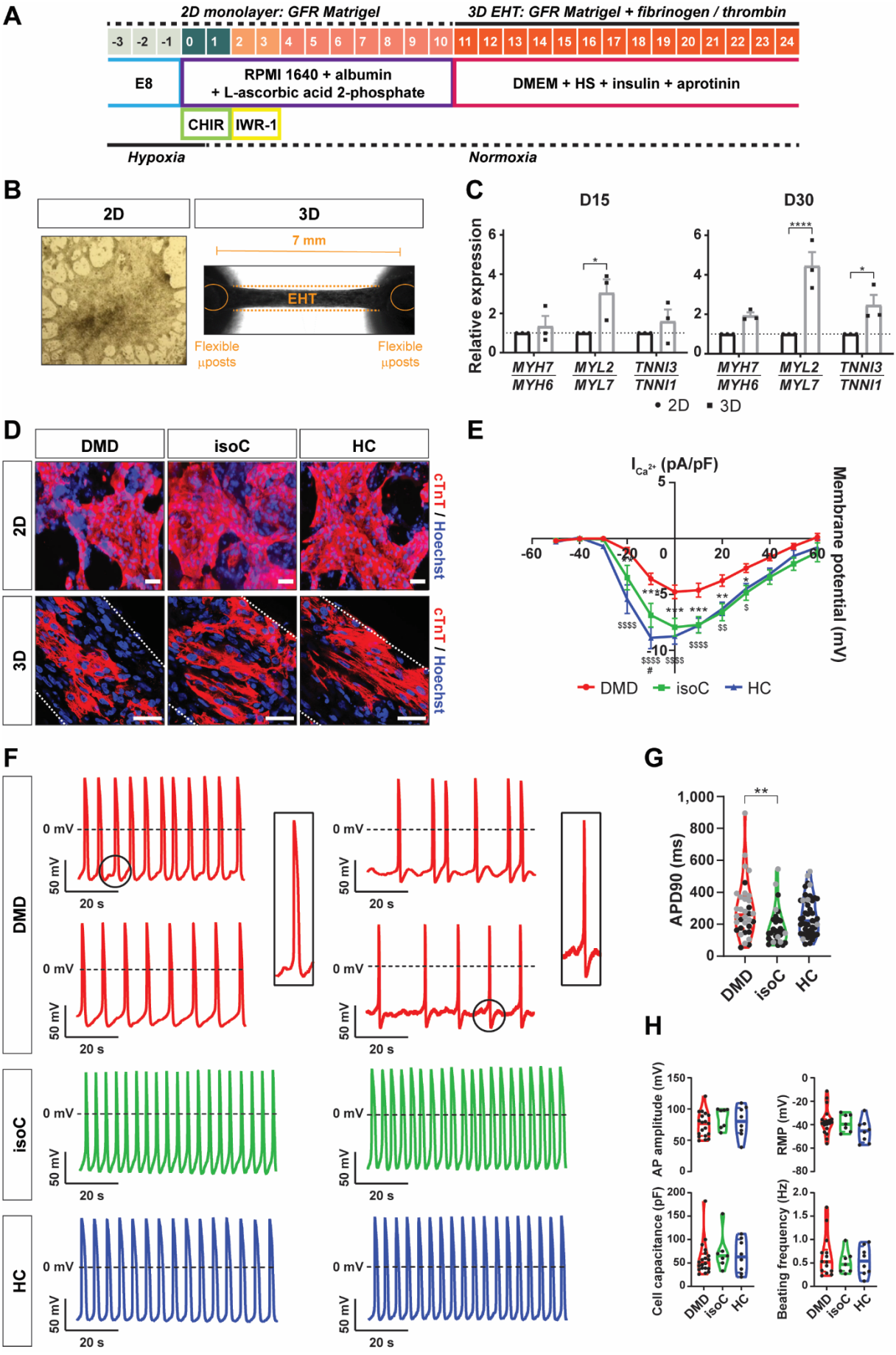

**Fig. 2: Characterization of the iPSC-CM differentiation protocol. (A)** Schematic representation of the cardiac differentiation protocol. Human iPSCs were differentiated to CMs in a monolayer cardiac differentiation protocol, using chemical Wnt signaling mediators (CHIR99021 and IWR-1), and, eventually, further matured into 3D EHT constructs based on fibrinogen and thrombin polymerization. **(B)** Representative example of 2D monolayer-based cardiac differentiation (*left panel*) and 3D mini-EHT construct between two flexible microposts, positioned 7 mm from each other (*right panel*). **(C)** Normalized gene expression ratios for isoforms of *Myosin Heavy Chain* (*MYH7/MYH6*), *Myosin Light Chain* (*MYL2/MYL7*) and *Cardiac Troponin I* (*TNNI3/TNNI1*) after 15 and 30 days of differentiation. Data were representative of three independent experiments (N = 3) and values were expressed as mean ± SEM. Significance of the difference was indicated as follows: *P < 0.05; **P < 0.01; ***P < 0.001 and ****P < 0.0001. **(D)** Immunostaining of Cardiac Troponin C (cTnT) positive CMs (cTnT, red and Hoechst, blue) in monolayer-based cardiac differentiation (2D) or EHT constructs (3D). White dotted lines indicated the borders of the 3D EHT constructs. Scale bar: 50 μm. **(E)** Voltage-current relation curve of the L-type $Ca^{2+}$ current (pA/pF), assessed after whole-cell patch-clamp configuration. Data were representative of three independent experiments (N = 3; DMD: n = 13, DMD isogenic: n = 7, healthy: n = 11) and values were expressed as mean ± SEM. Significance of the difference was indicated as follows: *P < 0.05; **P < 0.01; ***P < 0.001 and ****P < 0.0001 (DMD vs. DMD isogenic control); or $^{\$}$P < 0.05; $^{\$\$}$P < 0.01; $^{\$\$\$}$P < 0.001 and $^{\$\$\$\$}$P < 0.0001 (DMD vs. healthy control). **(F)** Representative AP recordings from DMD and control iPSC-CMs. DMD iPSC-CMs displayed arrhythmogenic firing pattern including DADs and OPPs. **(G)** Patch-clamp recordings at day 24 of differentiation for mean APD90 (ms). Additional measurements were performed with di-4-ANEPPS (gray dots). **(H)** Patch-clamp recordings for AP amplitude (mV), RMP (mV), cell capacitance (pF) and beating frequency (Hz). Data were representative of three independent

experiments (N = 3; DMD: n = 19, DMD isogenic: n = 7, healthy: n = 8). Significance of the difference was indicated as follows: *P < 0.05; **P < 0.01; ***P < 0.001 and ****P < 0.0001.

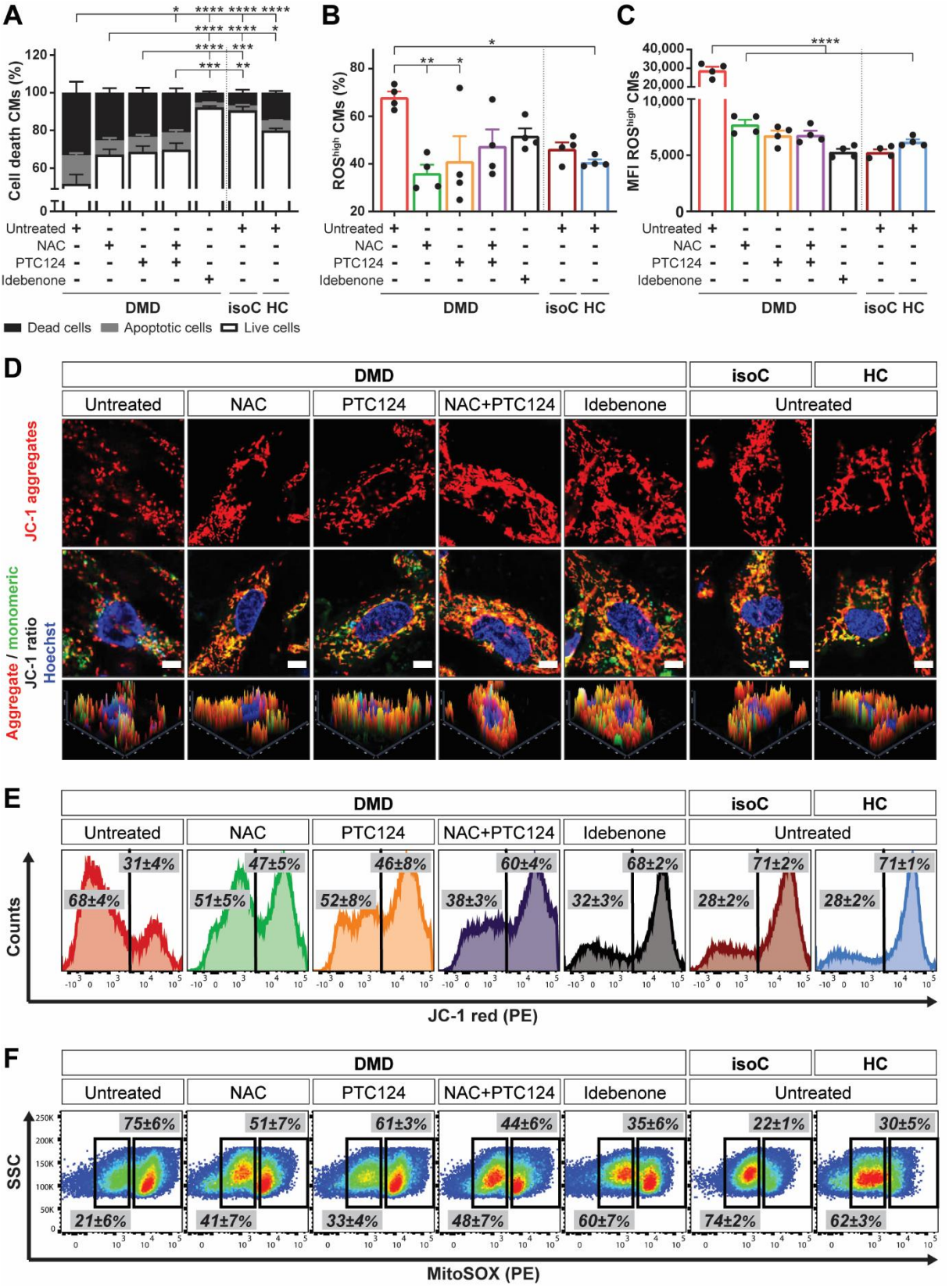


**Fig. 3: Characterization of the cardiomyopathic phenotype *in vitro* of DMD iPSC-CMs, showing premature cell death, depolarized mitochondria and increased intracellular ROS levels, which were counteracted by NAC, ataluren (PTC124) and idebenone.** Flow

cytometric quantification at day 15 of cardiac differentiation showing the percentage of cell death of Signal-Regulatory Protein Alpha (SIRPA) positive iPSC-CMs **(A)**, the percentage of CMs with high intracellular ROS levels **(B)** and the MFI of intracellular ROS in CMs **(C)** in conditions with (NAC, PTC124 and idebenone) or without (untreated) treatments. Data were representative of four independent experiments (N = 4) and values were reported as mean ± SEM. Significance of the difference was indicated as *P < 0.05; **P < 0.01; ***P < 0.001 and ****P < 0.0001. **(D)** Immunostaining of the fluorescent voltage-sensitive dye JC-1 was used to determine $\Delta\Psi_m$ and mitochondrial health in 15-day-old differentiated iPSC-CMs. Untreated DMD iPSC-CMs were characterized by mitochondrial depolarization, as indicated by the decrease in mitochondrial aggregates (JC-1 red, *upper panels*) and the increase in mitochondrial monomers (JC-1 green, *middle panels*) in respect to treated DMD iPSC-CMs and controls. Corresponding histograms (*lower panels*) showed the JC-1 fluorescence intensity ratios (aggregates/monomers). Scale bar = 5 μm. **(E)** Representative flow cytometric analyses at day 15 of differentiation for JC-1 aggregates (PE) and JC-1 monomers (FITC) in DMD iPSC-CMs upon treatment. Data were representative of four independent experiments (N = 4). **(F)** Flow cytometric analyses at day 15 of differentiation showing the mitochondrial superoxide production (MitoSOX, PE) in depolarized DMD mitochondria compared to DMD isogenic and healthy controls. Data were representative of four independent experiments (N = 4). Flow cytometry data were reported as mean ± SEM.

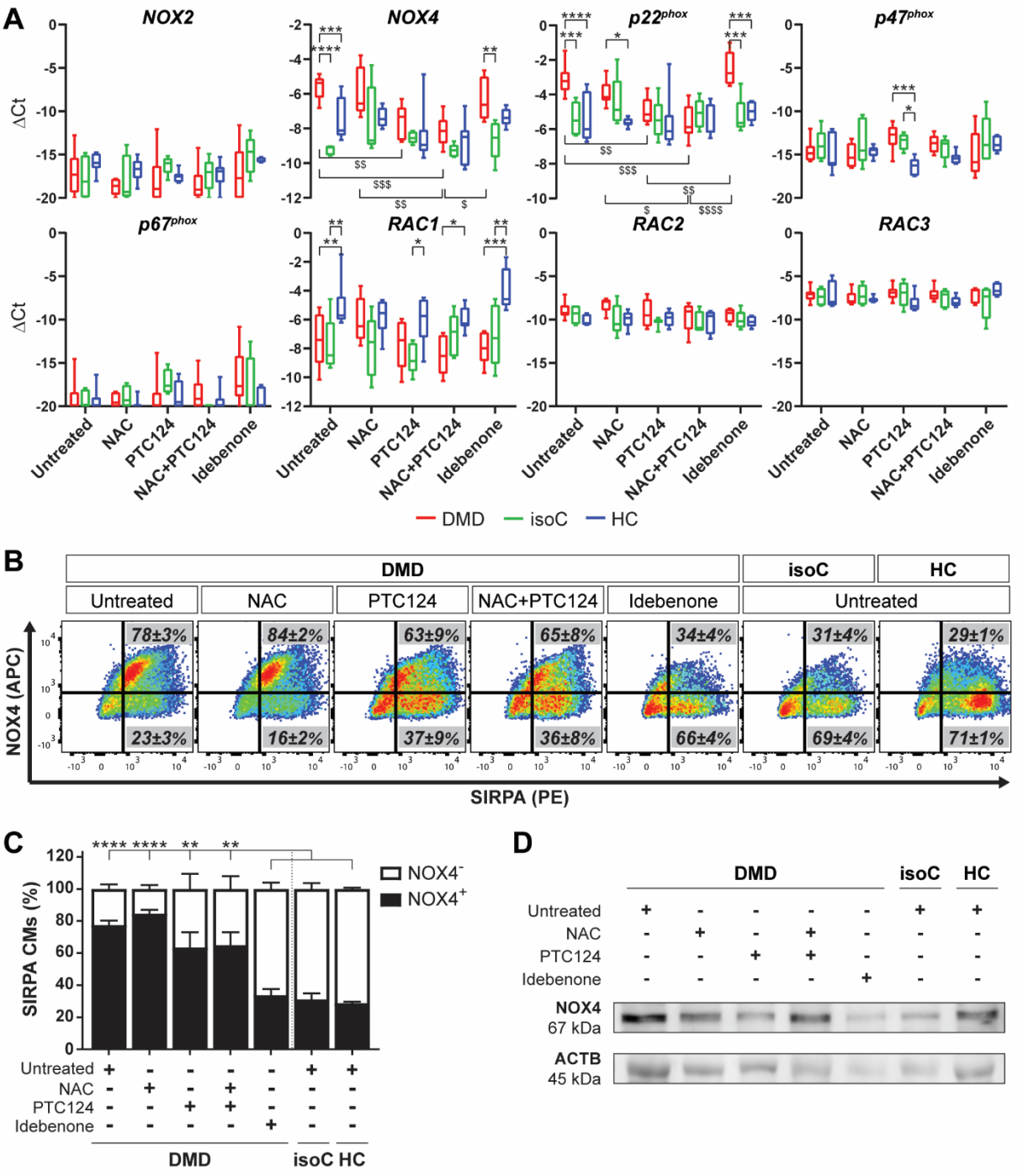


**Fig. 4: Increased expression levels of the ROS-producing NOX family enzyme NOX4 and its accessory regulatory subunit p22$^{phox}$ in Dystrophin-Deficient iPSC-CM cultures. (A)** Gene expression profiles at day 24 of cardiac differentiation of *NOX2* and *NOX4*, and the regulatory subunits (*p22$^{phox}$*, *p47$^{phox}$*, *p67$^{phox}$*, *RAC1*, *RAC2* and *RAC3*) in DMD, DMD isogenic and healthy control iPSC-CMs upon treatment with NAC, PTC124 and idebenone. Each data point was represented as ΔCt, normalized for the housekeeping genes (*GAPDH* and *RPL13a*).

Data were representative of five or more independent experiments (N ≥ 5) and values were expressed as mean ± SEM. Significance of the difference was indicated as follows: *P < 0.05; **P < 0.01; ***P < 0.001 and ****P < 0.0001 vs. subjects within the treatment condition; or $^{\$}$P < 0.05; $^{\$\$}$P < 0.01; $^{\$\$\$}$P < 0.001 and $^{\$\$\$\$}$P < 0.0001 vs. treatment conditions within the subject group. **(B)** Representative flow cytometric analyses at day 15 of differentiation showing the percentage of NOX4 (APC) protein expression in SIRPA (PE) positive DMD iPSC-CMs upon treatment. Data were representative of three independent experiments (N = 3). Flow cytometry data were reported as mean ± SEM. **(C)** Flow cytometric quantification at day 15 of differentiation of the percentage of SIRPA positive iPSC-CMs expressing NOX4 upon treatment. Data were representative of three independent experiments (N = 3) and values were expressed as mean ± SEM. Significance of the difference was indicated as follows: *P < 0.05; **P < 0.01; ***P < 0.001 and ****P < 0.0001. **(D)** Western blot analysis quantifying the protein expression levels of NOX4 in 15-day-old differentiated DMD and control iPSC-CMs, normalized to the loading protein ACTB.

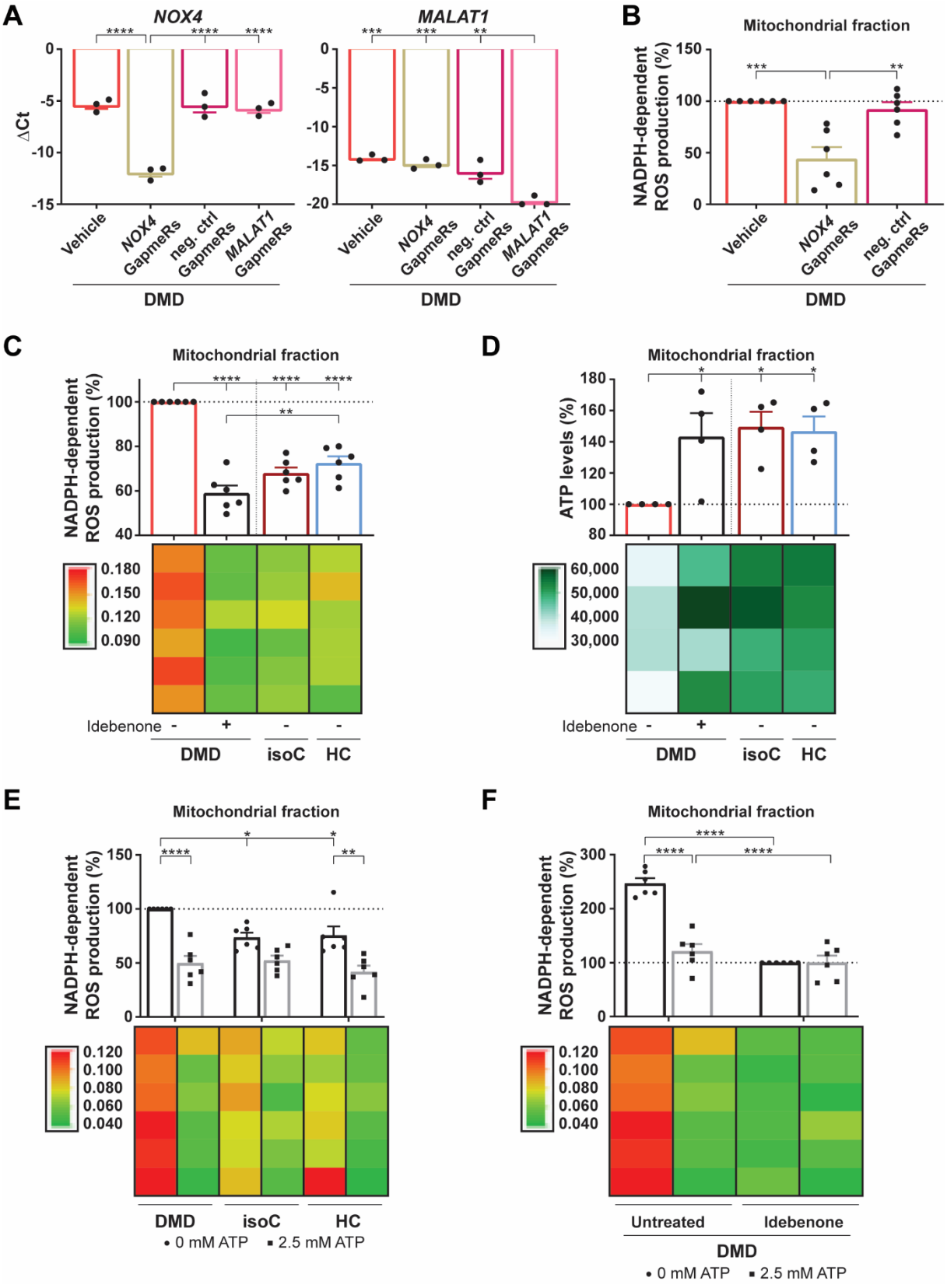


**Fig. 5: Idebenone could counteract the oxidative stress in DMD iPSC-CMs through ATP stimulation of the mitochondrial ETC, which, on its turn, reduced ROS-producing NOX4**

**activity. (A)** Quantitative RT-PCR of *NOX4* gene expression levels after the addition of NOX4 targeted Antisense LNA GapmeRs to the DMD iPSC-CM cultures (*left panel*). As positive control for the efficiency of the Antisense LNA GapmeRs, *MALAT1* levels were determined after the addition of MALAT1 targeted Antisense LNA GapmeRs to the DMD iPSC-CM cultures (*right panel*). Each data point was represented as ΔCt, normalized for the housekeeping genes (*GAPDH* and *RPL13a*). Data were representative of three independent experiments (N = 3) and values were expressed as mean ± SEM. Significance of the difference was indicated as follows: *P < 0.05; **P < 0.01; ***P < 0.001 and ****P < 0.0001. **(B)** Quantification of the NOX4-mediated ROS production, measured via the NADPH-dependent ROS generation, in the isolated mitochondrial fraction of DMD iPSC-CMs after a 6 days preincubation with GapmeRs, inducing *NOX4* mRNA transient degradation. Each data point was represented as percentage (%), normalized to the mitochondrial fraction of the untreated DMD iPSC-CMs (vehicle). **(C)** Quantification of the NADPH-dependent ROS production of NOX4 in the mitochondrial fraction of DMD iPSC-CMs with or without idebenone treatment compared to DMD isogenic and healthy controls. **(D)** ATP luminescence detection showing the effect of idebenone treatment on the mitochondrial ATP levels in DMD iPSC-CMs. **(E)** Quantification of the ROS-producing NOX4 activity after 2.5 mM ATP addition in DMD iPSC-CM and control cultures. Each data point was represented as percentage (%), normalized to the mitochondrial fraction of the untreated DMD iPSC-CMs. **(F)** Quantification of the NADPH-dependent ROS production of NOX4 in the mitochondrial fraction of DMD iPSC-CMs upon 2.5 mM ATP addition, with or without idebenone treatment. Each data point was represented as percentage (%), normalized to the mitochondrial fraction of the idebenone-treated DMD iPSC-CM cultures. Data were representative of four or six independent experiments (N = 4 or N = 6) and values were expressed as mean ± SEM. Colored rectangles represented the independent experiments.

1055 Significance of the difference was indicated as follows: *P < 0.05; **P < 0.01; ***P < 0.001

1056 and ****P < 0.0001.

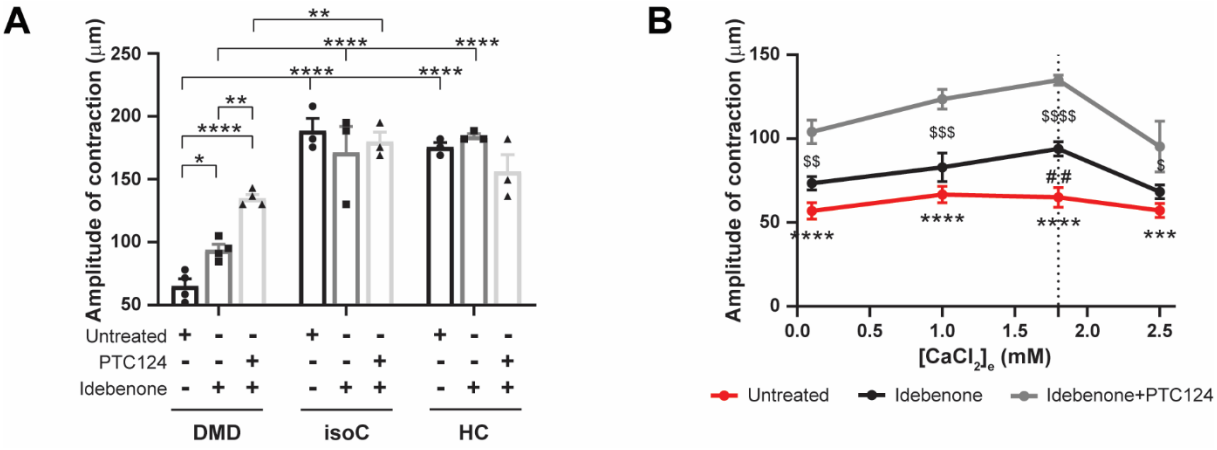


**Fig. 6: Improved contraction of 3D EHT constructs after administration of idebenone alone or idebenone in combination with PTC124 under physiological $Ca^{2+}$ levels. (A)** Spontaneous contraction and relaxation cycles of EHTs were monitored under temperature-controlled conditions (37°C) at 1.8 mM physiological $Ca^{2+}$ concentrations, and measured by the deflection movements of the microposts (in µm). The effect of idebenone and PTC124 on the contractility of EHTs derived from DMD iPSC-CMs (EHT diameter in µm: 1,041.9 ± 74.1) was compared to DMD isogenic (diameter in µm: 938.0 ± 86.6) and healthy control EHTs (diameter in µm: 849.9 ± 80.5). Data were representative of three or four independent experiments (N ≥ 3) and values were expressed as mean ± SEM. Significance of the difference was indicated as follows: *P < 0.05; **P < 0.01; ***P < 0.001 and ****P < 0.0001. **(B)** EHTs derived from DMD iPSC-CMs were incubated with various $Ca^{2+}$ concentrations (ranging from 0.1 to 2.5 mM) to assess the amplitude of contraction. Data were representative of three or four independent experiments (N ≥ 3) and values were expressed as mean ± SEM. Significance of the difference was indicated as follows: *P < 0.05; **P < 0.01; ***P < 0.001 and ****P < 0.0001 (untreated vs. idebenone+PTC124); or $^{\$}P < 0.05; $^{\$\$}P < 0.01; $^{\$\$\$}P < 0.001 and $^{\$\$\$\$}P < 0.0001 (idebenone vs. idebenone+PTC124); or $^{\#}P < 0.05; $^{\#\#}P < 0.01; $^{\#\#\#}P < 0.001 and $^{\#\#\#\#}P < 0.0001 (untreated vs. idebenone).